# USING PAIR-CORRELATION FUNCTION AS A TOOL TO IDENTIFY THE LOCATION FOR SHALE GAS/OIL RESERVOIR BASED ON THE EXPERIMENTAL WELL LOG DATA

---

A Thesis Presented to

the Faculty of the Department of Earth and Atmospheric Sciences

University of Houston

---

In Partial Fulfillment

of the Requirements for the Degree

Master of Science

in

Geophysics

---

By

Feifei Huang

December 2013

**USING PAIR-CORRELATION FUNCTION AS A TOOL TO IDENTIFY THE LOCATION FOR SHALE GAS/OIL RESERVOIR BASED ON THE EXPERIMENTAL WELL LOG DATA**

**Feifei Huang**

APPROVED:

**Dr. Evgeny M. Chesnokov, Chairman**

**Dr. Aibing Li**

**Dr. Donald Kouri**

**Dr. Aslan Gassiyev**

**Dean, College of Natural Sciences and Mathematics**

# ACKNOWLEDGEMENTS

I would like to thank my advisor Dr. Evgeny M. Chesnokov and my committee members, Dr. Aibing Li, Dr. Donald Kouri and Dr. Aslan Gassiyev, for their guidance and useful remarks and corrections.

Dr. Evgeny M. Chesnokov, my dissertation supervisor, has provided guidance and contributed many valuable suggestions to this dissertation. I really appreciate his patient instruction on this thesis. I am very thankful to Dr. Aibing Li for her advice and comments that helped to improve this paper. I also want to thank Dr. Donald Kouri for his useful comments, advice, and encouragement in my study. Special thanks extend to Dr. Aslan Gassiyev for his help and technical support on the UPs software program.

# USING PAIR-CORRELATION FUNCTION AS A TOOL TO IDENTIFY THE LOCATION FOR SHALE GAS/OIL RESERVOIR BASED ON THE EXPERIMENTAL WELL LOG DATA

---

An Abstract of a Thesis

Presented to

the Faculty of the Department of Earth and Atmospheric Sciences

University of Houston

---

In Partial Fulfillment

of the Requirements for the Degree

Master of Science

in

Geophysics

---

By

Feifei Huang

December 2013

# ABSTRACT

Shale gas reservoirs, as unconventional resources, are becoming an increasingly important exploration, development, and production target in the oil industry. However, geophysical characterization of these unconventional reservoirs remains challenging because of poor understanding of geophysical responses to reservoir properties.

Pair-correlation function is determined as a product of fluctuations of random functions at two arbitrary points. Based on the experimental data from four different wells, I calculated the pair-correlation function and its relative parameter: amplitude-correlation value. The results showed that the productive layers have high pair-correlation value and non-productive layers have a low correlation value and suggest that amplitudes of pair-correlation function reflect the level of the difference between the inclusions and the material rocks, so the increasing of the organic content generally enhances the amplitude of pair correlation. Hence, the results of these calculations show the potential applications of pair-correlation function and its amplitude for the detection of the productive layers.

Therefore, we can use pair-correlation function and its amplitude as a tool to predict the location for shale gas/oil reservoir and to estimate the thickness of productive layer in productive well. Furthermore, we also can use amplitude of pair-correlation function with elasticity tensor components and Vp/Vs ratio to distinguish the productive wells from non-productive wells.

# Content

ACKNOWLEDGEMENTS ..... iii
ABSTRACT ..... v
List of tables ..... viii
List of Figures ..... ix
Chapter 1 Introduction ..... 1
1.1 Importance of Shale ..... 1
1.2 Motivation ..... 3
1.3 Overview of Thesis ..... 4
Chapter 2 Geological Background and Data Set ..... 5
2.1 Barnett Shale ..... 5
2.2 Experimental data from wells ..... 7
Chapter 3 Definition of Pair-correlation Function and its Parameters ..... 9
3.1 Definition of pair correlation function ..... 9
3.2 Definition of the amplitude of pair-correlation function ..... 10
3.3 Definition of correlation radius of pair-correlation function ..... 10
Chapter 4 Method for Pair-correlation Function from Standard Sonic Data ..... 11
4.1 Idea of pair-correlation function ..... 11
4.2 Theory of pair-correlation function ..... 12
4.3 Method of pair-correlation function ..... 16
4.3.1. Average method used for pair-correlation function calculation ..... 16
4.3.1. a. Simple-average method ..... 16
4.3.1.b. Running-window approach ..... 17
4.3.1.c. Dynamic-window-average method ..... 18
4.3.2. Elasticity tensor calculation used for pair-correlation function ..... 20
4.3.2.a. Specific elasticity tensor ..... 20
4.3.2.b. Averaged elasticity tensor ..... 21
4.3.2.c. Fluctuation elasticity tensor ..... 22
4.3.3. Pair-correlation function for the elasticity tensor components and density ..... 22
Chapter 5 Result and Analysis ..... 24
5.1. Pair-correlation function as a tool for distinguishing productive and nonproductive layers ..... 24
5.1.1 Results of the pair-correlation function in the productive layer ..... 24
5.1.2 Results of the pair-correlation function in nonproductive layer ..... 26
5.1.3 Comparison of the pair-correlation function in productive and nonproductive layers ..... 26
5.2. Amplitude of pair-correlation function versus depth ..... 30
5.2.1 Using amplitude of pair-correlation function to identify the location of productive layers in productive well (Well 1) ..... 30
5.2.1 Using amplitude of pair-correlation function to distinguish productive wells from nonproductive wells ..... 32
5.2.1.a. Comparison of the amplitudes of the pair-correlation function for elasticity modules and density in a productive well (Well 1) and a nonproductive well (Well 2) ..... 32
5.2.1.b Comparison of the amplitudes of the pair-correlation function for elasticity modules

and density in productive well (Well 1) and nonproductive wells (Well 3 and Well 4) .....34
5.3 Frequency-dependent amplitude of the pair-correlation function in productive well (Well 1) .....39
Chapter 6 Summary .....43
References .....46

# List of tables

Table 2-1: Experimental data from wells .....7

# List of Figures

Figure 1: Number of producing Barnett Shale wells versus time. Pitts Oil Company, Dallas Production Inc. (Martineau, 2007).....2
Figure 2: Barnett Shale producing counties in the Fort Worth Basin. Source: Humble Geochemical, Pickering Energy Partners (Lu, 2012).....5
Figure 3: Generalized stratigraphy section– Fort Worth Basin showing the distribution of the source, reservoir, and seal rocks of the Barnett- Paleozoic total petroleum system (TPS). (Montgomery, 2005).....6
Figure 4: The figure shows the located depth of the Barnett Shale for Well 1 according to its sonic log data.....7
Figure 5: Graphs show the experimental data from Well 1. Plots include: (a) Vp velocity verse depth; (b) density versus depth; (c) $Vs1$ versus depth; (d) $Vs2$ versus depth.....8
Figure 6: Representation of random heterogeneous media. The white background is the matrix rock, and the green solid circles are the inclusion in the matrix. The double-ended arrows specify the interaction between two arbitrary points in the space (Tiwary, 2009).9
Figure 7: Frequency-dependent anisotropy versus frequency and angles. The maximum value of anisotropy (6%) is reached as frequency is zero, while the value of anisotropy is close to zero when the frequency is equal to 0.6 kHz (Chesnokov, 2001).....12
Figure 8: The average values are calculated by simple-average method of Vp data from Well 1.....16
Figure 9: Schematic of the running-window concept. The center of the dashed window with length $L1$ is shown by a dark solid circle and the window size is $L1$. Then the window moves downward to the next location, symbolized by a dotted window with length $L2$ and its center is shown by the next lower dark circle (Tiwary, 2009).....17
Figure 10: Averaged values of Vp calculated by using the dynamic-window-average method. (a) Averaged Vp with the window size in 250 Hz; (b) averaged Vp with the window size in 500 Hz; (c) averaged Vp with the window size in 1000 Hz; (d) averaged Vp with the window size in 2000 Hz.....19
Figure 11: Elasticity properties of Barnett Shale calculated based on the experimental data from Well 1. Figure includes: (a) $C33$ versus depth; (b) $C44$ versus depth.....21
Figure 12: Pair-correlation functions for diverse elements of elasticity tensor and density constructed at 7140 ft depth, which is a productive layer. Vp is 15222 ft/s; Vs1 is 8726 ft/s. Frequency is 250 Hz.....25
Figure 13: Pair-correlation functions for diverse elements of elasticity tensor and density constructed at 7420 ft depth, which is a nonproductive layer. Vp is 12054 ft/s; Vs1 is 7552 ft/s. Frequency is 250 Hz.....27
Figure 14: Correlation function is $< C33, C33, >$and frequency is 250 Hz: in (a) and (c), red lines represent the productive layers (Depth 7140 ft and Depth 7130 ft); in (b) and (d), the blue lines represent nonproductive layers (Depth 7420 ft and Depth 7280 ft).....28

Figure 15: Correlation function is <C44′ C44′ > and frequency is 250 Hz: in (a) and (c), the red lines are productive layers (Depth 7140 ft and Depth 7130 ft); in (b) and (d) the blue lines are non productive layers (Depth 7420 ft and Depth 7280 ft). .....29
Figure 16: Amplitudes of pair-correlation function for the Barnett Shale based on the experimental log data from Well 1. Frequency is 250 Hz. (a) Amplitude of pair-correlation function $< \mathrm{VP}, \mathrm{VP}, >$. (b) Amplitude of pair-correlation function $< \rho' \ \rho' >$. (c) Amplitude of pair-correlation function $< \mathrm{Vs1}, \mathrm{Vs1}, >$. (d) Amplitude of pair-correlation function $< Vs2, Vs2, >$. (e) Amplitude of pair-correlation function $< \mathrm{C33}, \mathrm{C33}, >$. (f) Amplitude of pair-correlation function $< C44, C44, >$. .....31
Figure 17: Amplitudes of pair-correlation function for elasticity modules and density of the Barnett Shale based on the experimental log data from Well 1 and Well 2. Frequency is 250 Hz. (a.1) Amplitude of pair-correlation function $< \mathrm{C33}, \mathrm{C33}, >$ for Well 1. (b.1) Amplitude of pair-correlation function $< \mathrm{C33}, \mathrm{C33}, >$ for Well 2. (a.2) Amplitude of pair-correlation function $< C44, C44, >$ for Well 1. (b.2) Amplitude of pair-correlation function $< C44, C44, >$ for Well 2. (a.3) Amplitude of pair-correlation function $< \rho' \ \rho' >$ for Well 1. (b.3) Amplitude of pair-correlation function $< \rho' \ \rho' >$ for Well 2. .....33
Figure 18: Amplitudes of pair-correlation function for elasticity modules and density of the Barnett Shale based on the experimental log data from Well 1 and Well 3. The frequency is 250 Hz. (a.1) Amplitude of pair-correlation function $< \mathrm{C33}, \mathrm{C33}, >$ for Well 1. (b.1) Amplitude of pair-correlation function $< \mathrm{C33}, \mathrm{C33}, >$ for Well 3. (a.2) Amplitude of pair-correlation function $< C44, C44, >$ for Well 1. (b.2) Amplitude of pair-correlation function $< C44, C44, >$ for Well 3. (a.3) Amplitude of pair-correlation function $< \rho' \ \rho' >$ for Well 1. (b.3) Amplitude of pair-correlation function $< \rho' \ \rho' >$ for Well 3. .....35
Figure 19: Amplitudes of pair-correlation function for elasticity modules and density about the Barnett Shale based on the experimental log data from Well 1 and Well 4. Frequency is 250Hz. (a.1) Amplitude of pair-correlation function $< \mathrm{C33}, \mathrm{C33}, >$ for Well 1. (b.1) Amplitude of pair-correlation function $< \mathrm{C33}, \mathrm{C33}, >$for Well 4. (a.2) Amplitude of pair-correlation function $< C44, C44, >$ for Well 1. (b.2) Amplitude of pair-correlation function $< C44, C44, >$ for Well 4. (a.3) Amplitude of pair-correlation function $< \rho' \ \rho' >$ for Well 1. (b.3) Amplitude of pair-correlation function $< \rho' \ \rho' >$ for Well 4. .....36
Figure 20: Amplitudes of pair-correlation function for Vp/Vs ratio about the Barnett Shale based on the experimental log data from productive well (Well 1) and nonproductive wells (Well 3 and Well 4). Frequency is 250 Hz. (a.1) Amplitude of pair-correlation function for Well 1. (b.1) Amplitude of pair-correlation function for Well 3. (a.2) Amplitude of pair-correlation function for Well 1. (b.2) Amplitude of pair-correlation function for Well 4.....38
Figure 21: Amplitudes of pair-correlation function $< \mathrm{C33}, \mathrm{C33}, >$ for the Barnett Shale based on the experimental log data from Well 1. (a) Amplitude of pair-correlation function $< \mathrm{C33}, \mathrm{C33}, >$ at 100 Hz. (b) Amplitude of pair-correlation function $< \mathrm{C33}, \mathrm{C33}, >$ at 150 Hz. (c) Amplitude of pair-correlation function $< \mathrm{C33}, \mathrm{C33}, >$ at 250 Hz. (d) Amplitude of pair-correlation function $< \mathrm{C33}, \mathrm{C33}, >$ at 500 Hz. (e)

Amplitude of pair-correlation function $< C33, C33, >$ at 1000 Hz. (f) Amplitude of pair-correlation function $< C33, C33, >$ at 2000 Hz. .....40
Figure 22: Amplitude of pair-correlation function $< C33, C33, >$ for productive well (Well 1) in the frequency scale (100 Hz to 1000 Hz). .....41
Figure 23: Amplitude of pair-correlation function $< C33, C33, >$ in diverse frequency (100 Hz, 150 Hz, 250 Hz, 500 Hz, 1000 Hz, 2000 Hz) for a certain depth. The red line represents the productive layer-7140 ft; the blue line symbolizes the nonproductive layer-7420 ft. Solid circled points stand for amplitude value for each given frequency. 42

# Chapter 1 Introduction

## 1.1 Importance of Shale

Shale is fine-grained, organic-rich, elastic rock characterized by thin layers of clays and silts. They are the most common sedimentary rocks (Pettijohn, 1975).

In petroleum geology, organic shale is seal rock that traps oil and gas as well as source rocks. As a type of source rock, shale gas reservoir has yielded and expulsed hydrocarbons to more porous and permeable strata by various procedures and mechanisms, and also retained a portion of the hydrocarbon generated during the geological period (Glorioso, 2012). Shale can be considered as the source, reservoir and seal for unconventional natural gas.

While much U.S. natural gas production comes from conventional resources, unconventional gas reservoirs such as gas-shale reservoirs and tight-gas sands are becoming important petroleum exploration targets as a result of their gas storage capacities and potential for large recoverable resource (Ross, 2008). The development of shale gas reservoirs exploration benefits from the application and advancements in water fracturing and horizontal drilling technologies. The number of producing wells in the Barnett Shale (the Newark East field) is shown in Figure 1. From 1981 to 1990, only 100 wells were completed. Between 1991 and 1996, there were 275 new wells completed. After 1997, more than 5829 wells were drilled, completed and put on

production (Martineau, 2007).

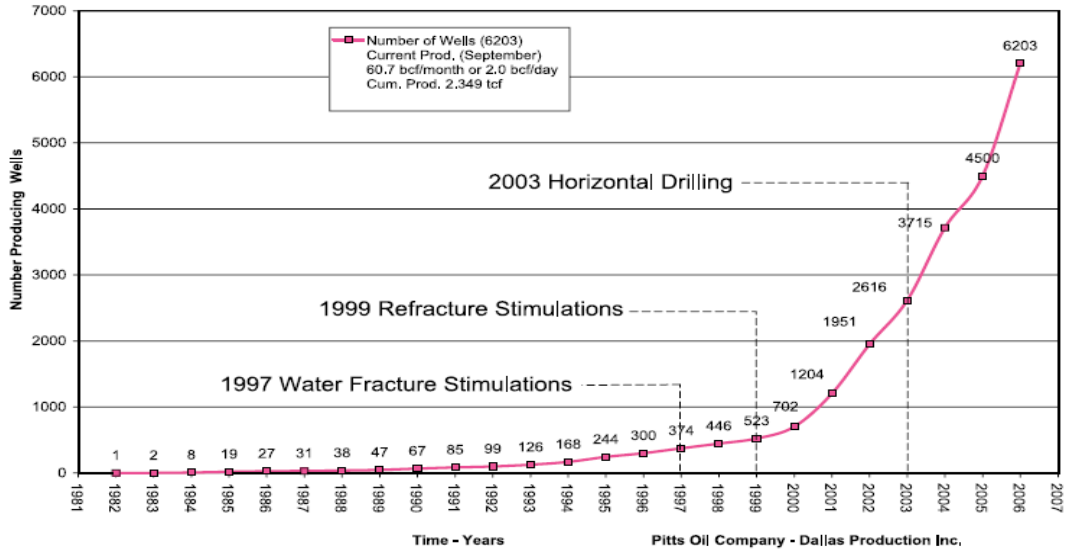


Figure 1: Number of producing Barnett Shale wells versus time. Pitts Oil Company, Dallas Production Inc. (Martineau, 2007).

As a potentially large resource for future gas production, shale gas is garnering increasing attention from both academic and industrial circles. Despite having quite different geologic settings, many shale-gas formations share features such as low matrix porosity, low permeability, and brittleness. Economic shale-gas development candidates require ample organic matter to generate sufficient volumes of hydrocarbons, i.e., relatively high total organic carbon (TOC). The complexity of shale-gas formations has prompted geophysicists to attempt to establish a basis of knowledge and experience about production from different disciplines, such as geology, seismic, and rock physics. Most of the knowledge on shale gas reservoir prediction has been obtained from analyzing sedimentological, stratigraphic, geochemical, and rock physical data (e.g., Leckie et al., 1990; Slatt and O'brien, 2011; Slatt and Abousleiman, 2011).

## 1.2 Motivation

Shale gas reservoirs are considered unconventional gas resources. As unconventional gas reservoirs, shale has different features from sandstone. For example, shale has lower porosity and permeability than sandstone. Therefore, most traditional technologies that detect the gas reservoir cannot be applied to shale, such as AVO behavior and cross-session analysis between the density log and neutron log.

This begs the question: can geophysical well-logging data provide a method for shale gas reservoir prediction? In this thesis, pair correlation function will be used as a tool to predict the location for the shale gas reservoir. Investigation of frequency-dependent anisotropy is significant for us in understanding the internal structure of shale reservoir, in addition to recognizing the procedures for the construction of those structures. Dr. Evgeni M. Chesnokov developed the mathematical techniques of pair-correlation function to calculate the dynamic frequency-dependent effective physical characteristics of porous cracked anisotropic media. This method is derived from the expansions of elasticity modulus fluctuations into the Fourier series and applied for experimental seismic data (Chesnokov, 2002). This algorithm transforms the compressional velocity (Vp), shear velocities (Vs) and densities ($\rho$) versus the depth to the calculations of the amplitudes of the correlation functions versus the depth. By calculating the amplitude of pair-correlation from a suite of log measurements, geophysical responses of shale-gas rocks will be analyzed to predict properties of shale. The results demonstrate that the existence of large amplitude values of the correlation functions reflect the enhanced inhomogeneity at a

certain depth. Moreover, the other independent methods also prove that these depths are oil and gas locations (Chesnokov, 2002).

Generally, the motivation of this thesis is to determine the layer depth of the shale gas reservoirs and recognize the productive wells by applying the pair-correlation function method to borehole data recorded in some vertical wells penetrating a shale formation (the Barnett Shale).

## 1.3 Overview of Thesis

This thesis is separated into six parts. Chapter 1 gives the introduction and motivation of this paper. Chapter 2 describes the geological background and experimental data of wells. Chapter 3 introduces the definition of pair-correlation function. Chapter 4 demonstrates the method of pair-correlation function. Chapter 5 reports the results calculated and the analysis of all the calculations, and in the final chapter, Chapter 6, discusses the conclusions.

# Chapter 2Geological Background and Data Set

## 2.1 Barnett Shale

The shale gas reservoir studied in this thesis is the Barnett Shale, which come from the Fort Worth Basin in North Central Texas (Figure 2). It is one of the largest and most active domestic natural gas plays in the U.S.

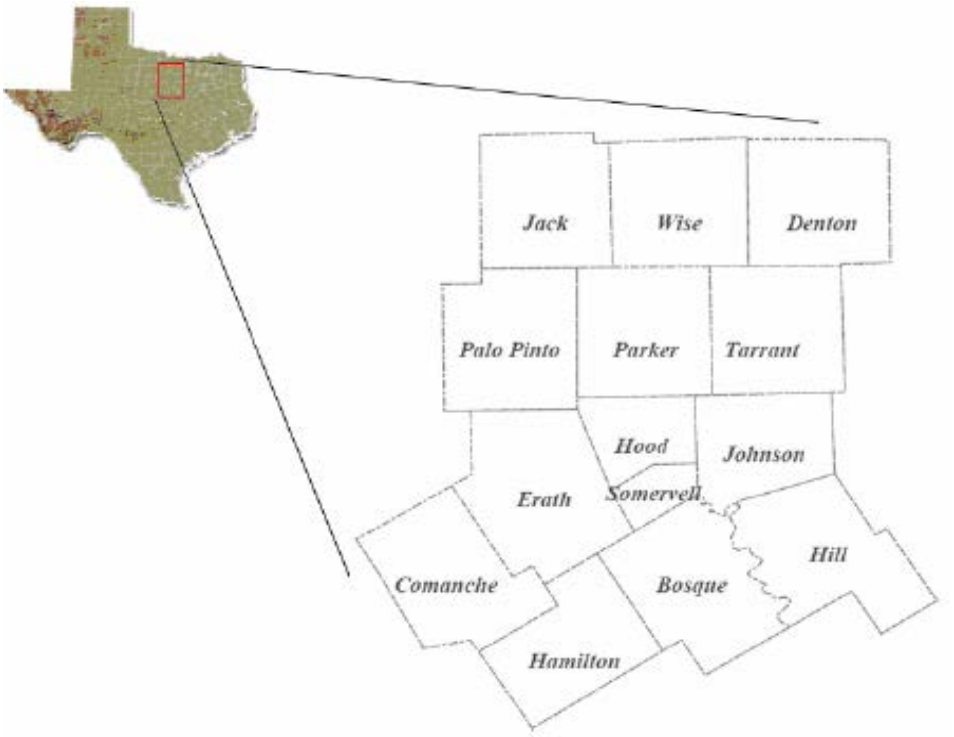


Figure 2: Barnett Shale producing counties in the Fort Worth Basin. Source: Humble Geochemical, Pickering Energy Partners (Lu, 2012).

The Mississippian Barnett Shale is an organic-rich black shale. Commonly, it is located at depths of 6,500-8,500 feet deep. Figure 3 displays the generalized stratigraphy of the Fort Worth Basin. Toward southwest, the Barnett Shale lies between two limestone units, the underlying Mississippian-age Chappel Limestone and the overlying Pennsylvanian-age Marble Falls Limestone. Heading northeast, the

thickness of Barnett Shale increases and the underlying unit becomes Ordovician-age Viola Limestone. The Barnett Shale is divided into the upper and lower Barnett by the Forestburg Limestone (Montgomery, 2005).

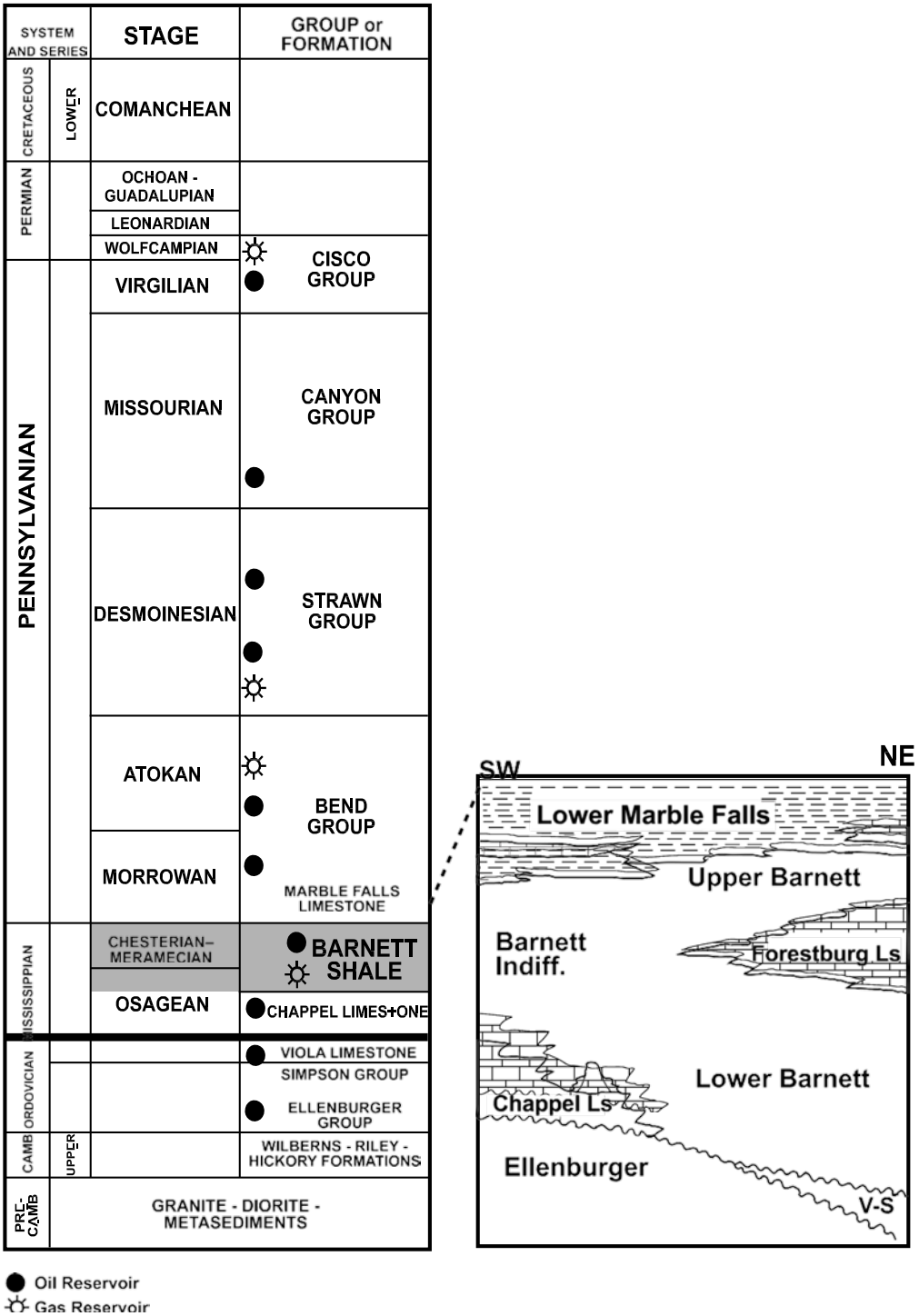


Figure 3: Generalized stratigraphy section– Fort Worth Basin showing the distribution of the source, reservoir, and seal rocks of the Barnett- Paleozoic total petroleum system (TPS). (Montgomery, 2005)

## 2.2 Experimental data from wells

The experimental data in this thesis was recorded from 4 wells (Table2-1). Well 1 is a productive well, located at the Fort Worth basin. According to the analysis from the Grammy log data, the depth of the Barnett Shale covers from 7000ft to 7500 ft, which is our considered depth (Figure 4). Its sonic data is dipole sonic data, including $Vs_1$ and $Vs_2$. The velocities, densities and porosities of the data from Well 1 are shown in Figure 5.Well 2, 3 and 4 are non-productive wells.

Table 2-1: Experimental data from wells

| Well No. | Name | Productive | Depth Scale (ft) | Log Data |
|---|---|---|---|---|
| Well 1 | DT_4 | Yes | 7000-7500 | Vp, $Vs_1$, $Vs_2$, Density |
| Well 2 | AD_2 | No | 7300-7500 | Vp, Vs, Density |
| Well 3 | BS_4 | No | 7000-7500 | Vp, Vs, Density |
| Well 4 | EP_4 | No | 7000-7500 | Vp, Vs, Density |

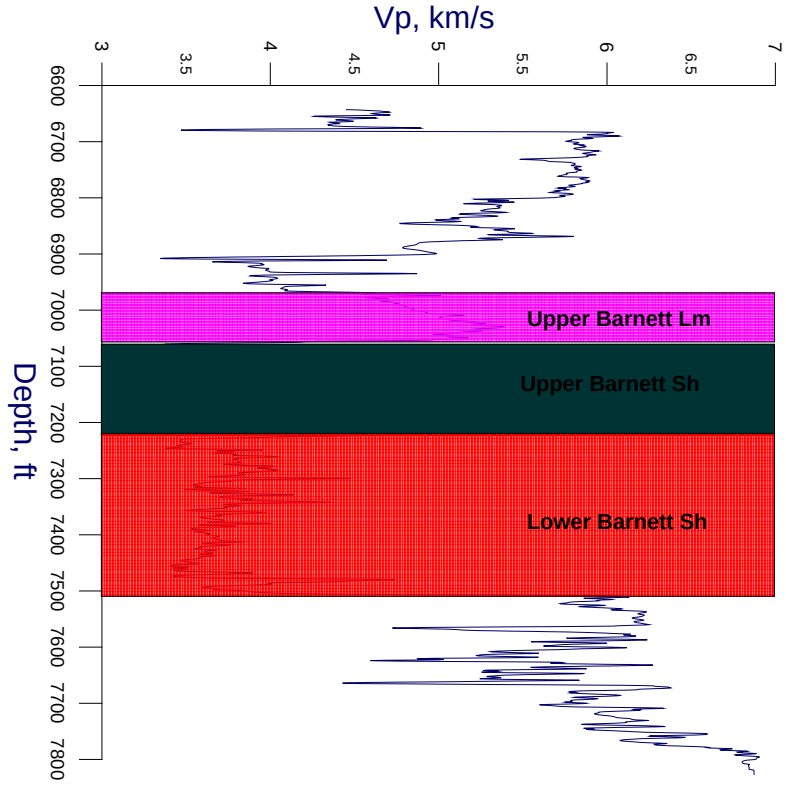


Figure 4: The figure shows the located depth of the Barnett Shale for Well 1 according to its sonic log data.

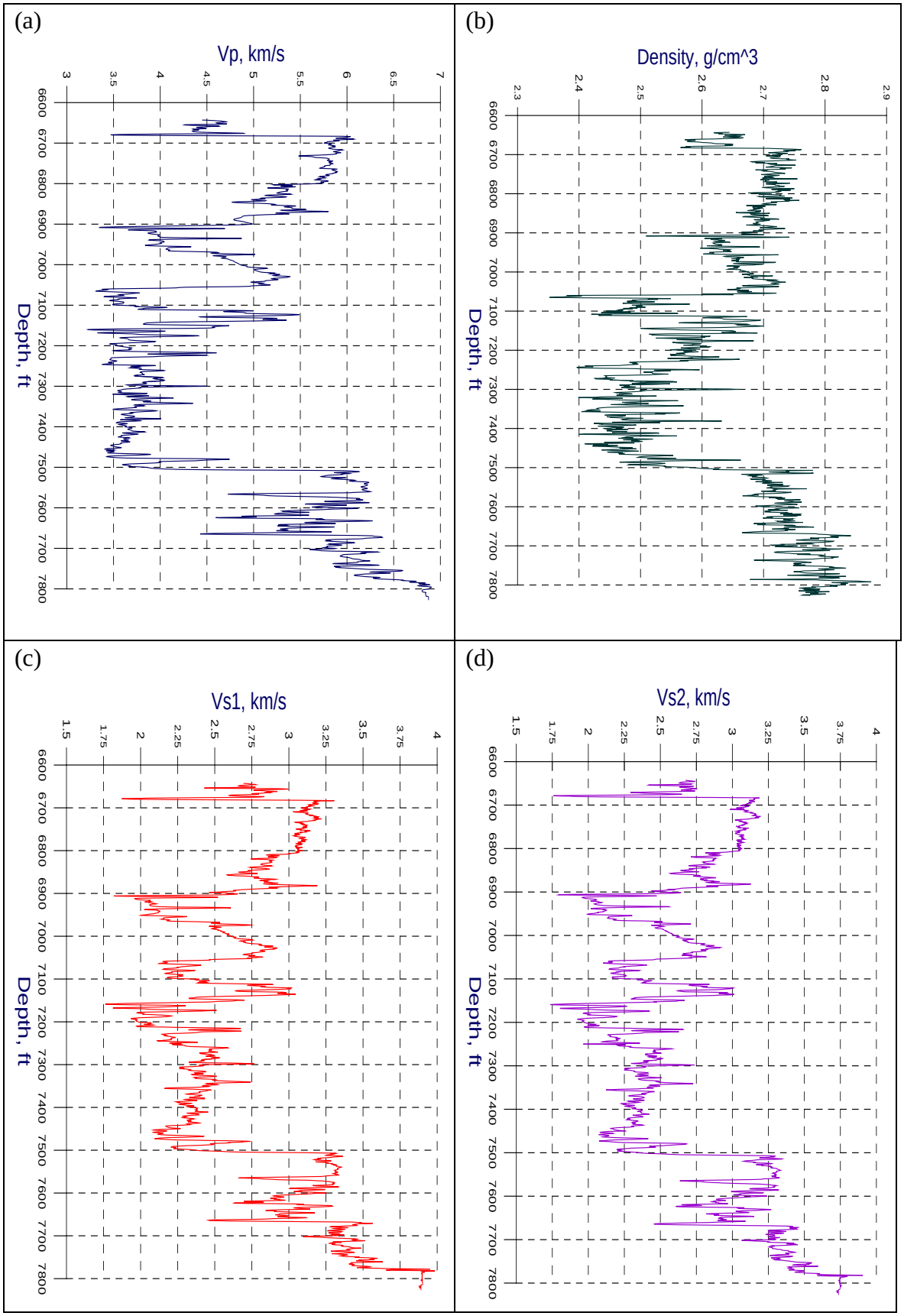


Figure 5: Graphs show the experimental data from Well 1. Plots include: (a) Vp velocity verse depth; (b) density versus depth; (c) $Vs_1$ versus depth; (d) $Vs_2$ versus depth.

# Chapter 3 Definition of Pair-correlation Function and its Parameters

## 3.1 Definition of pair correlation function

Pair-correlation function is determined as a product of fluctuations of random fluctuations at two arbitrary points (Chesnokov, 2001). Pair-correlation function was developed by Dr. Chensnokov as a method to calculate the frequency-dependent elasticity tensor of a heterogeneous medium and to investigate frequency-dependent anisotropy. This method considers the interactions between two of the arbitrary points of a heterogeneous medium. Figure 6 shows a schematic of interactions in a heterogeneous medium. Hence, pair-correlation function method can be applied to estimate a frequency-dependent elastic tensor for the heterogeneous medium.

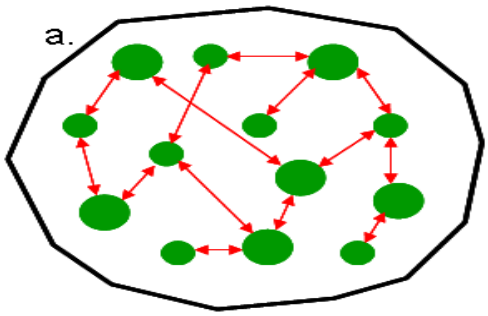


Figure 6: Representation of random heterogeneous media. The white background is the matrix rock, and the green solid circles are the inclusion in the matrix. The double-ended arrows specify the interaction between two arbitrary points in the space (Tiwary, 2009).

Its basic formula (Bayuk, Ammerman, and Chesnokov, 2008) is

$$B(r_1, r_2) = <C'(r_1) \cdot C'(r_2)>, \quad (3\text{-}1)$$

which is determined by fluctuations of random layered medium.

## 3.2 Definition of the amplitude of pair-correlation function

One of the main purposes of this study is to find out two significant factors of correlation function: amplitude and correlation radius. The amplitude of pair-correlation function is defined as the function value at zero argument, when argument difference r equals zero. In this case, the value is "maximum and equals to dispersion of the random function" (Chesnokov, 2001). According to definition, the formula for amplitude of the correlation function is determined as follows:

$$\text{Ac=B(0)=}<C'(r), C'(r)>|_{Window} = \frac{1}{L_w}\int_0^{L_w} C'(r)\, C'(r) dr. \quad (3\text{-}2)$$

## 3.3 Definition of correlation radius of pair-correlation function

An important characteristic of the random process is correlation radius. The correlation radius means that the values are independent from each other at distances greater than correlation radius, $r^{corr}$. The correlation function radius illustrates the rate of correlation function reduction while the absolute value of argument increases. Therefore, the correlation radius is determined as follows (Chesnokov, 2011):

$$\text{Rc=}\frac{3}{4\pi B(0)}\int_0^{L_w} |B(r)|\, dr, \quad (3\text{-}3)$$

where $B(r)$ is the three dimension correlation function. When averaging with the moving window, reliable values can only be obtained if the correlation radius is smaller than the window size.

# Chapter 4 Method for Pair-correlation Function from Standard Sonic Data

## 4.1 Idea of pair-correlation function

Generally, when the wavelength of the waves propagating in the medium is much greater than the size of inclusions, the ordered medium can be considered anisotropic. It means that "anisotropy can only be observed when the wavelengths of propagating waves (P or S) are much greater than at least one (of possibly many) scale lengths associated with the sizes of inhomogeneity, i.e., in the case where the assumptions of the long wavelength approximation are satisfied"(Chesnokov, 2001 and Liu, 2003). The reasons that cause inhomogeneity include variations of lithology, pore fluid and saturation porosity (Roy, 2001).

Pair-correlation function is developed by Dr. Chesnokov et. al. in 2001 to investigate the frequency-dependent anisotropy for heterogonous medium and to understand the interior structure of rocks. Their previous studies not only prove that anisotropy of the heterogeneous medium will vary with the changing of the frequency, but also indicate that the position of enhanced heterogeneities matches the location of shale gas/oil reservoir. The results of their studies in Figure 7 prove that pair-correlation function can be used to investigate the frequency-dependent anisotropy, which will decrease with the increase of frequency (Chesnokov, 2001).

Therefore, in this thesis, we need to test that pair-correlation function and its amplitude are frequency dependent as well as frequency-dependent anisotropy, and to

show that the maximum amplitude in low frequency corresponds to the enhanced heterogeneity caused by gas/oil inclusion. Hence, we can use pair-correlation function to identify the location of shale gas/oil reservoir. We also can use the amplitude of pair-correlation function to estimate the thickness of the productive layers and to distinguish the productive wells from nonproductive wells.

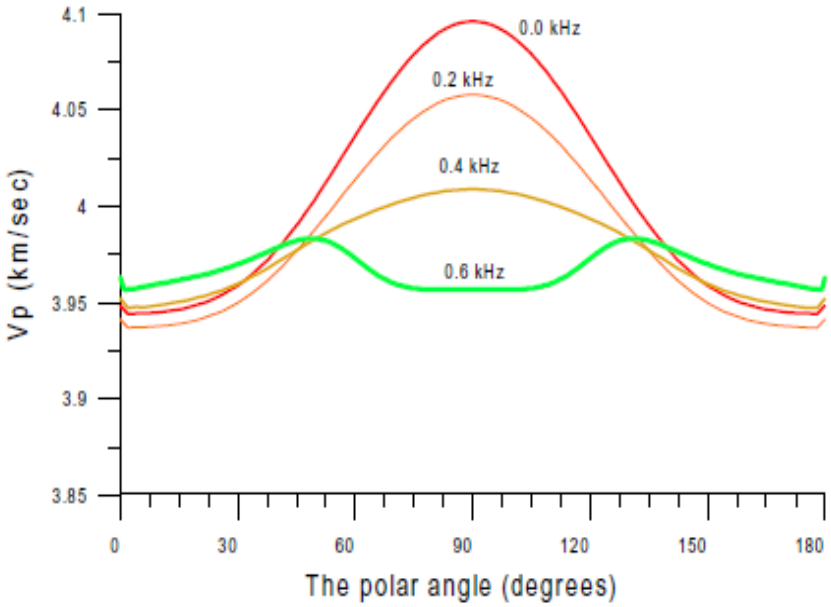


Figure 7: Frequency-dependent anisotropy versus frequency and angles. The maximum value of anisotropy (6%) is reached as frequency is zero, while the value of anisotropy is close to zero when the frequency is equal to 0.6 kHz (Chesnokov, 2001).

## 4.2 Theory of pair-correlation function

The formula for the wave equation for random elastic media without initial stress is (Chesnokov, 1998; Roy, 2001):

$$L_{ik}(x)U_k(x) = f_i(x). \tag{4-1}$$

The expression of operator L is:

$$L_{ik}(x) = -\delta_{ik}\rho(x)\frac{\partial^2}{\partial t^2} + \nabla_j C_{ijkl}\nabla_l. \tag{4-2}$$

According to the formula, operator L depends on the factors of random media $\rho(x)$ and $C_{ijkl}(x)$. We assume that

$$\rho(x) =< \rho > +\rho'(x) \text{ and } C_{ijkl} =< C > +C'_{ijkl}(x). \quad (4\text{-}3)$$

By substituting formulas (4-3) into (4-2), we can get the new formula for L as:

$$L_{ik}(x) =< L_{ik}(x) > +L'_{ik}(x). \quad (4\text{-}4)$$

The formula for the solution of wave equation (4-1) is:

$$U_i(t,x) = \int G_{ik}(t-t_1, x-x_1)\, f_k(x_1,t_1) dx_1 dt_1 \quad (4\text{-}5)$$

After substituting the formula (4-5) into (4-1), we can derive the equation for Green function, G:

$$L_{ik}(x) G_{kj}(t-t_1, x-x_1) = -\delta_{ij}\delta(t-t_1)\delta(x-x_1). \quad (4\text{-}6)$$

So the averaged displacement <$U$> can be written by the averaged Green function < $G$>:

$$< U_i(t,x) >= \int < G_{ik}(t-t_1, x-x_1) > f_k(x_1,t_1) dx_1 dt_1. \quad (4\text{-}7)$$

Then we can get the Dyson equation by averaging Green function and introducing the mass operator M (Chesnokov and Kukharenko, 1997; Chesnokov et al., 1995, 1998; Chesnokov et al., 2000; Roy, 2001):

$$< G_{ik}(t-t_1, x-x_1) >= G^0_{ik}(t-t_1, x-x_1) + \int dt_2 dt_3\, dx_2 dx_3 G^0_{ik}(t-t_2, x-x_2)$$
$$M_{km}(t_2-t_{3,}x_2-x_3) < G_{km}(t_2-t_{3,}x_2-x_3) >. \quad (4\text{-}8)$$

The operator M in equation (4-8) can be expressed as a summation of four mass operators, which reveals the interactions between different parameters, like "moduli-moduli", "moduli-density" and "density-density". Then we can express the

Dyson equation (4-8) in terms of $\omega, k$ by applying the Fourier transformation (Roy, 2001):

$$\left[\omega^2\rho^*(\omega,k)\delta_{ik} - C^*_{ijkl}(\omega,k)k_jk_l\right]G_{kn}(\omega,k) = -\delta_{kn}. \quad (4\text{-}9)$$

where $C^*_{ijkl}$and $\rho^*$ are effective elastic moduli and density; and $k_j$ is a component of the wave vector.

The frequency-dependent tensors of elastic components and density are calculated based on the formulas (Shermergor, 1977; Chesnokov et al., 1995, 1996, 1998, 2000, 2001):

$$C^*_{ijkl}(\omega,k) = < C_{ijkl}(r) > + \int \cos(k,r)\left[\frac{\partial}{\partial x_n}\frac{\partial}{\partial x_q}G^0_{mp}(\omega,r)\right]{}^{(cc)}_{B^{pqkl}_{ijmn}}(r)dr; \quad (4\text{-}10)$$

$$\rho^*(\omega,k) = < \rho(r) > -\omega^2 \int \cos(k,r)\, G^0_{ik}(\omega,r)\, {}^{(\rho\rho)}_{B}(r)dr, \quad (4\text{-}11)$$

where $\omega$ is the cyclic frequency, k is the wave vector, $\frac{\partial}{\partial x_n}\frac{\partial}{\partial x_q}G^0_{mp}(\omega,r)$ is the second derivative of the Green function, and $G^0$ is the dynamic Green's tensor, which depends on the medium's properties and frequency. The equation for dynamic Green's tensor can be expressed as (Tiwary, 2009):

$$G^0_{ij}(\omega,r) = \frac{1}{r}\left[h(\omega,r)\delta_{ij} + g(\omega,r)\frac{x_ix_j}{r^2}\right]; \quad (4\text{-}12)$$

$$h(\omega,r) \equiv \frac{1}{4\pi\rho\omega^2r^2}\{[(1+\frac{ir\omega}{V})e^{-i\omega r/V}]^{V_p}_{V_s} + \frac{r^2\omega^2}{V_s^2}e^{-i\omega r/V_s}\}; \quad (4\text{-}13)$$

$$g(\omega,r) \equiv \frac{1}{4\pi\rho\omega^2r^2}\{\left[3\left(1+\frac{ir\omega}{V}\right) - \frac{r^2\omega^2}{V^2}\right]e^{-\frac{i\omega r}{V}}\}^{V_p}_{V_s}. \quad (4\text{-}14)$$

Here, $f(V)^{V_p}_{V_s} \equiv f(V_p) - f(V_s)$.

According to the formulas (4-10) and (4-11), the difference between the effective and average elastic components is determined by the second term. The previous research results show that the enhanced difference location correlates with the location of the productive layer. Roy et al. (2001) and Bayuk et al. (2003)

developed the pair-correlation function as a technology to predict elastic wave behavior from a variety of logging data with higher frequency.

Its basic formula (Bayuk, Ammerman, and Chesnokov, 2008) is

$$B(r_1, r_2) = <C'(r_1) \cdot C'(r_2)>, \tag{4-15}$$

which is determined by fluctuations of random layered medium.

$B^{(cc)}_{ijmn}{}^{pqkl}(r)$ and $B^{(\rho\rho)}_{}(r)$ are the pair-correlation functions of the fluctuations of elastic modules and density of the heterogonous medium and the formulas are:

$$B^{(cc)}_{ijmn}{}^{pqkl}(r) =< C'_{pqkl}(x)C'_{ijmn}(x+r) >= A^{pqkl}_{ijmn}\varphi(r) \tag{4-16}$$

$$B^{(\rho\rho)}_{}(r) =< \rho'(x)\rho'(x+r) > \tag{4-17}$$

where, the value in the angle brackets are the averaged value, $C'(r)$ and $\rho'(r)$ are the fluctuation value, and $\varphi(r)$ is a function which explains the coordinate dependency of the correlation function depending on the direction of anisotropic medium (Tiwary, 2009).

In order to apply the pair-correlation method to the well-log data, we need to find:

1. averaged values and fluctuation values of the elasticity tensor;
2. correlation functions for density and for the elasticity tensor components;
3. parameters of correlation function: amplitude and correlation radius.

## 4.3 Method of pair-correlation function

### 4.3.1. Average method used for pair-correlation function calculation

#### 4.3.1. a. Simple-average method

Simple-average is a method used to calculate average values of elastic properties of the layers in a fixed given scale. This is the Voigt isostrain method. We add the properties of each point together and then divide by the total number of the points. The formula for simple average is

$$<V_p>=\frac{1}{N_s}\sum_{r=1}^{N_s} V_p(r), \qquad (4\text{-}18)$$

where the angle brackets indicate statistical averaging because of the medium we assumed as a statistically homogeneous medium. $N_s$ is the total number of the points in the given scale. For example, if the length of a given scale is 100 ft and the logging step is 0.5ft, there are 200 points in this window. $V_p(r)$ is the specific compressional velocity for the $r^{th}$ point. Figure 8 demonstrates the average values calculated by the simple-average method of Vp data from Well 1.

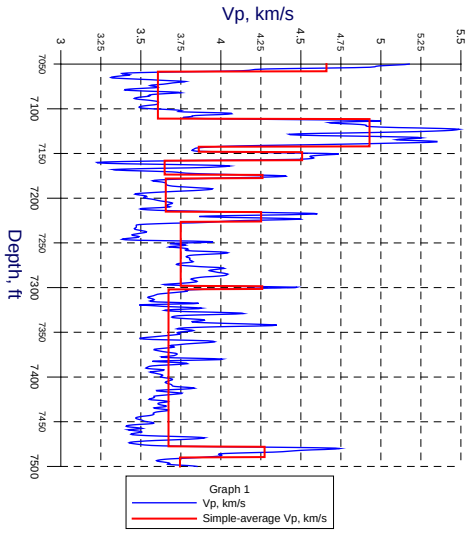


Figure 8: The average values are calculated by simple-average method of Vp data from Well 1.

### 4.3.1.b. Running-window approach

Running-window approach is a method using a moving window instead of a fixed given scale to complete the calculation. Within a window, the length of the window is equal to the distance between the first and last measurements and the averaged value calculated based on all of the data. After the calculation is finished at the given depth and the relative result is assigned at the center of the window, the window moves down to next logging depth and the process is repeated (Figure 9). As a result, we gain the distribution of properties versus depth.

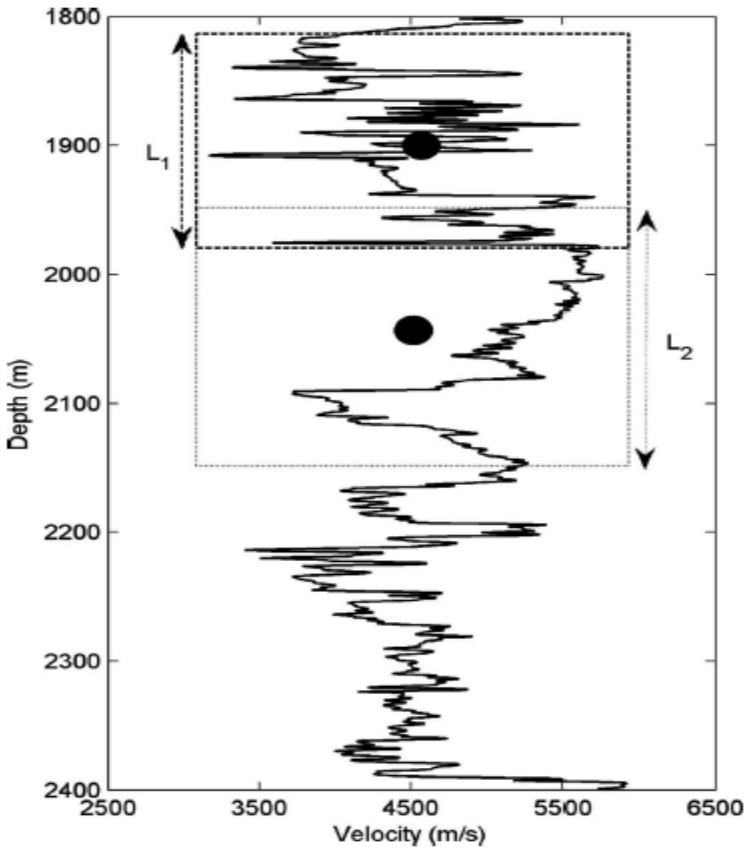


Figure 9: Schematic of the running-window concept. The center of the dashed window with length *L*1 is shown by a dark solid circle and the window size is *L*1. Then the window moves downward to the next location, symbolized by a dotted window with length *L*2 and its center is shown by the next lower dark circle (Tiwary, 2009).

### 4.3.1.c. Dynamic-window-average method

In this paper, we use the dynamic-window-average method, which combines the simple-average method with the running-window approach, to complete the calculation of the average properties of inhomogeneous layered medium. Instead of a given scale, the average value is calculated within a window size by the simple-average formula. Numerical tests prove that the results of the elastic tension determination become constant when the window size equals the wavelength for a given frequency. This creates a new formula:

$$<V_p> = \frac{1}{L_w}\sum_{r=1}^{L_w} V_p(r). \qquad (4\text{-}19)$$

Here, W is the running window and $L_w$ is the length of a window (Roy, 2001). The window length is based on the velocity of the elastic wave at a certain depth and the frequency we decided on, and the averaged result is assigned at the center of the window. The calculation of the moving window size based on the formula:

$$L_w = \lambda = V/f. \qquad (4\text{-}20)$$

Here, $L_w$ is window length, $\lambda$ is wavelength, V is velocity of elastic wave and f is frequency. Generally, the window size will change from a few feet to hundreds of feet, depending on the velocity at the given depth and the frequency, while the logging step remains at only 0.5 feet. This means that within the window size, there are enough large numbers of points for calculation, which also restricts the highest frequency for running-window approach in this paper being 2000 Hz. In this case, we assume the window is a frame whose length is equal to the wavelength for a given frequency. Furthermore, the frame length is also equal to the distance between the first and last

measurements of the well log data. We also assume that the $r$ point is the central point of the relative frame. In this case, half the length of the frame is $L_w/2$= (N-1)*logging step/2, here N is the total number in the window. As a result, we obtain a set of averaged values that depend on the depth. Figure 10 illustrates the averaged values of Vp data versus depth at various frequencies (250 Hz, 500 Hz, 1000 Hz, 2000 Hz).

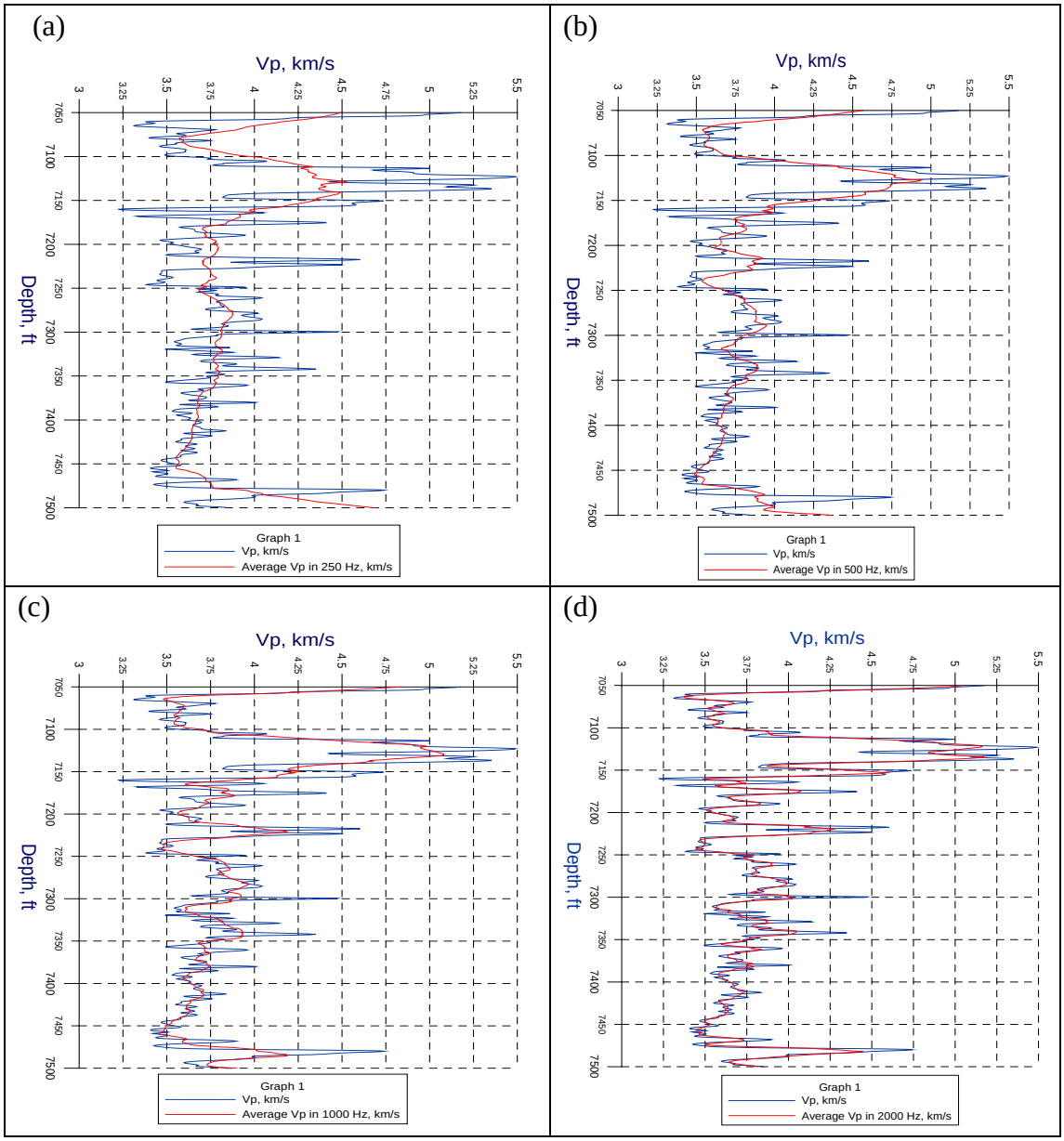


Figure 10: Averaged values of Vp calculated by using the dynamic-window-average method. (a) Averaged Vp with the window size in 250 Hz; (b) averaged Vp with the window size in 500 Hz; (c) averaged Vp with the window size in 1000 Hz; (d) averaged Vp with the window size in 2000 Hz.

Commonly, the lower frequency creates a larger window size, and the larger window size causes a smoother curve of the averaging values. Whereas the averaged values with a small window size based on a higher frequency correlate better with the real experimental data.

### 4.3.2. Elasticity tensor calculation used for pair-correlation function

#### 4.3.2.a. Specific elasticity tensor

In this thesis, we suppose that the experimental well log data, including elastic-wave velocity and density, are related to the whole layer between the logging depths. The thickness of each thin layer is considered to be equal to the logging step (0.5 ft). Normally, if we have the mineralogical composition at each depth, the stiffness tensor can be derived by some formulas (Bayuk et al, 2008). However, mostly these types of information are always unavailable. Generally, the rock's anisotropic properties cannot be predicted by the logging data (Vp, Vs and density $\rho$), so we assume that the medium has isotropic properties. Because we only have the vertical component of data at each logging depth, the specific stiffness tensor components at each point are calculated based on the experimental data Vp, Vs and density $\rho$ with the following formulas (Chesnokov, 2001):

$$C_{33}(r) = {V_p}^2(r)\rho(r); \tag{4-21}$$

$$C_{44}(r) = {V_s}^2(r)\rho(r). \tag{4-22}$$

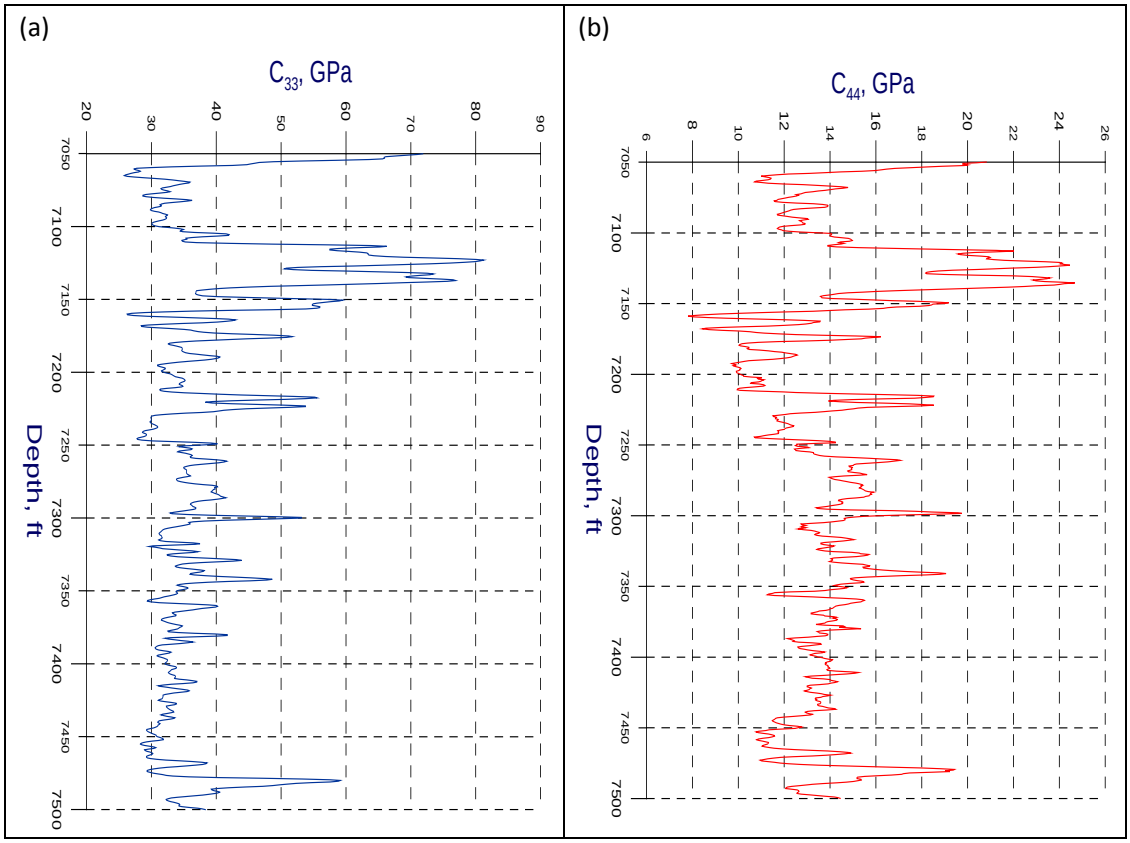


Figure 11: Elasticity properties of Barnett Shale calculated based on the experimental data from Well 1. Figure includes: (a) $C_{33}$ versus depth; (b) $C_{44}$ versus depth.

## 4.3.2.b. Averaged elasticity tensor

In order to gain the averaged elasticity characteristics dependent on depth, this thesis uses the dynamic-window-average method. According to formula 4-19 derived in section 4.3.1.c, we derive the formulas to calculate the averaged elasticity tensor:

$$<C_{33}>=\frac{1}{L_w}\sum_{r=1}^{L_w} C_{33}(r); \quad (4\text{-}23)$$

$$<C_{44}>=\frac{1}{L_w}\sum_{r=1}^{L_w} C_{44}(r); \quad (4\text{-}24)$$

Here W is the window and $L_w$ is the length of the window. Since the size of the window depends on the velocity and frequency, if we were to assign the same frequency for these elastic moduli, then the window size only depends on their related velocity at the r point. In other words, for the same frequency, the window size of $C_{33}$

depends on the velocity of its related compression wave, $V_p$. For $C_{44}$, it depends on the velocity of fast-shear wave, $V_s$.

### 4.3.2.c. Fluctuation elasticity tensor

The general definition of fluctuation is the deviation of the function from its averaged value. It means that the fluctuation $C'_{ii}(r)$ is the difference between the specific elasticity tensor at the point r and its related averaged value in a given window size. Therefore, according to its definition, for elasticity tensors at a point r of heterogeneous medium, the formulas of fluctuation are:

$$C'_{33}(r) = C_{33}(r) - < C_{33}(r) >; \quad (4\text{-}25)$$

$$C'_{44}(r) = C_{44}(r) - < C_{44}(r) >, \quad (4\text{-}26)$$

where $C'_{ii}(r)$ is the fluctuation stiffness tensor at the point r, $C_{ii}(r)$ is the relative specific stiffness tensor, and $< C_{ii}(r) >$ is the averaged value calculated by the dynamic-window-average method (Tiwary, 2008).

## 4.3.3. Pair-correlation function for the elasticity tensor components and density

After we obtain the fluctuation elasticity tensor, we can calculate the pair-correlation function for elasticity tensor components and density based on the formula 3-1 in section 3.1. When we consider the medium as statistically homogenous, the pair-correlation function formula 3-1 can be written as follows (Chesnokov, 2001):

$$\underset{B_{ijmn}^{pqkl}}{^{(cc)}}(r_1, r_2) \equiv \underset{B_{ijmn}^{pqkl}}{^{(cc)}}(r_1 - r_2) \equiv < C'_{ijkl}(r_1) C'_{pqmn}(r_2) >; \quad (4\text{-}27)$$

$$\underset{B}{^{(\rho\rho)}}(r_1, r_2) \equiv \underset{B}{^{(\rho\rho)}}(r_1 - r_2) \equiv < \rho'(r_1)\rho'(r_2) >. \quad (4\text{-}28)$$

Here, the pair-correlation function is only determined by the argument difference since it is a function of a single argument.

Then we apply the dynamic-window-average method to the pair-correlation function and calculate the averaged value over a domain window scale. The running window is a dynamic frequency-dependent window, because the widow size depends both on frequency and depth (Roy, 2001). Consequently, we develop the pair-correlation function in the following form (Chesnokov, 2002), assuming that $r = r_1 - r_2, r_1 = s + \frac{1}{2}r \; and \; r_2 = s - \frac{1}{2}r$:

$$\underset{B_{ijmn}^{pqkl}}{^{(cc)}}(r, s) = \frac{1}{Lw}\int_{-Lw/2}^{Lw/2} ds \;\; C'_{ijkl}(s + \tfrac{1}{2}r) C'_{pqmn}(s - \tfrac{1}{2}r); \quad (4\text{-}29)$$

$$\underset{B}{^{(\rho\rho)}}(r, s) = \frac{1}{Lw}\int_{-Lw/2}^{Lw/2} ds \;\; \rho'(s + \tfrac{1}{2}r)\rho'(s - \tfrac{1}{2}r), \quad (4\text{-}30)$$

where $Lw$ is the window length, $s$ is the middle point of the window.

In this thesis, the well-log data are discrete sets of points. Hereinafter, under the same assumption of the formulas 4-29 and 4-30, we derive the final formulas for the pair-correlation function as the below forms:

$$\underset{B_{ijmn}^{pqkl}}{^{(cc)}}(r, s) = \frac{1}{Nw}\sum_{Nw}[C_{ijkl}\left(s + \tfrac{1}{2}r\right) - < C_{ijkl} >]\,[C_{pqmn}\left(s - \tfrac{1}{2}r\right) - < C_{pqmn} >]; \quad (4\text{-}31)$$

$$\underset{B}{^{(\rho\rho)}}(r, s) = \frac{1}{Nw}\sum_{Nw}[\rho\left(s + \tfrac{1}{2}r\right) - < \rho >]\,[\rho\left(s - \tfrac{1}{2}r\right) - < \rho >]. \quad (4\text{-}32)$$

Here, $Nw$ is the total number of points in the window, and

$$Lw = (Nw - 1) * logging\ step, \text{ so}$$

$$Nw = 2\,Lw + 1 \text{ (logging step is 0.5 ft).} \quad (4\text{-}33)$$

# Chapter 5 Result and Analysis

According to the formulas for pair-correlation function in section 4.3.3, I wrote the program using Matlab software. Then I calculated the correlation values for the components of stiffness tensor and density for the Barnett Shale based on the experiment log data from Well 1. As a productive well, the Well 1 has both productive layers and nonproductive layers. Comparison of the results from both layers indicates that there are big differences between the correlation values of the productive layers and nonproductive layers.

## 5.1. Pair-correlation function as a tool for distinguishing productive and nonproductive layers

### 5.1.1 Results of the pair-correlation function in the productive layer

According to the other independent technologies, we know the depth of 7140 ft is a productive layer for Well 1. We complete the calculation of the pair-correlation function $<C'_{33}C'_{33}>$, $<C'_{44}C'_{44}>$ and $<\rho'\rho'>$for this layer. Here, the frequency we used is 250 Hz. $Vp$ is 15222 ft/s; $Vs_1$ is 8726 ft/s; $Vs_2$ is 8557 ft/s. Figure 12 represents the results of the calculation showing the maximum of $<C'_{33}C'_{33}>$ as 204.94 $GPa^2$; $<C'_{44}C'_{44}>$ is 8.7 $GPa^2$, and $<\rho'\rho'>$ is 0.005$(g/cm^3)^2$

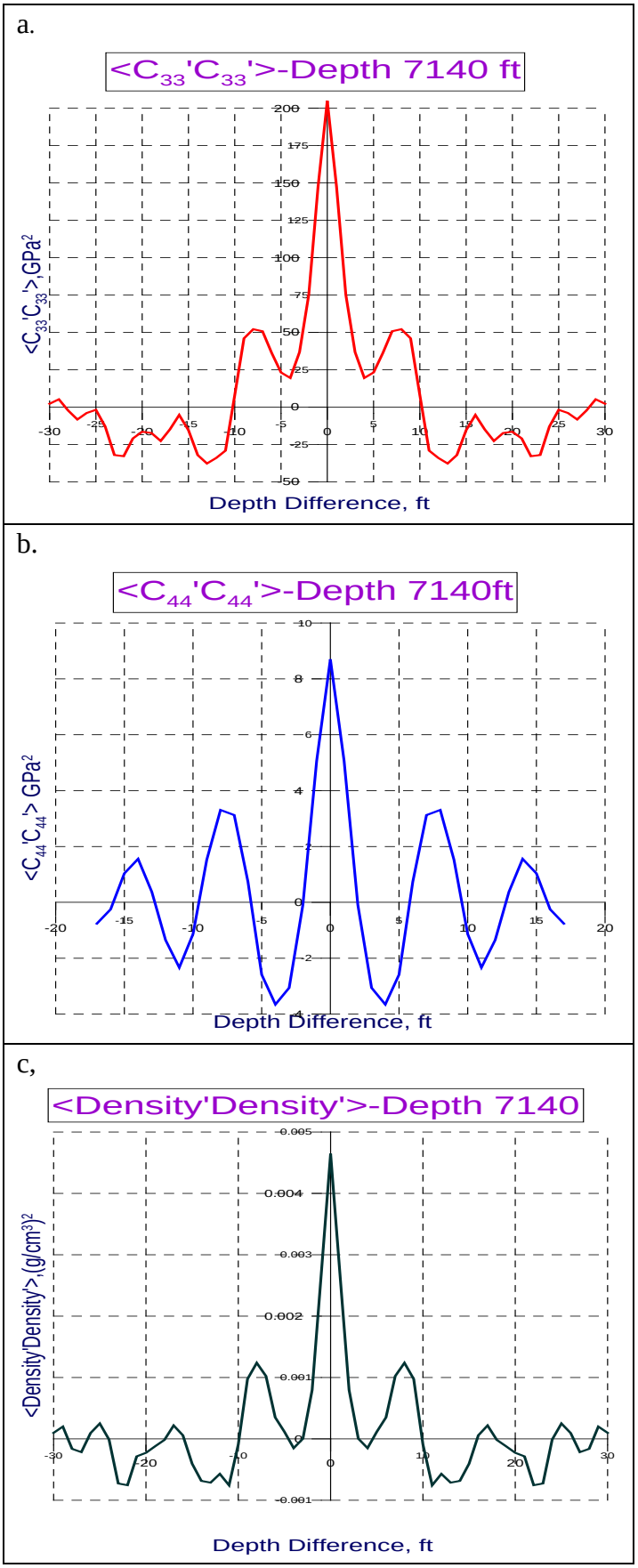


Figure 12: Pair-correlation functions for diverse elements of elasticity tensor and density constructed at 7140 ft depth, which is a productive layer. Vp is 15222 ft/s; $Vs_1$ is 8726 ft/s. Frequency is 250 Hz.

### 5.1.2 Results of the pair-correlation function in nonproductive layer

Based on the data from Well 1, we also calculate the pair-correlation function $<C'_{33}C'_{33}>$, $<C'_{44}C'_{44}>$ and $<\rho'\rho'>$ for the nonproductive layer with a depth of 7420 ft. Here, the frequency is still 250 Hz. $Vp$ is 12054 ft/s; $Vs_1$ is 7552 ft/s; $Vs_2$ is 7515 ft/s. The outcomes are shown in Figure 13. The maximum of $<C'_{33}C'_{33}>$ is 1.76 $GPa^2$; $<C'_{44}C'_{44}>$ is 0.37 $GPa^2$ and $<\rho'\rho'>$ is 0.001$(g/cm^3)^2$

### 5.1.3 Comparison of the pair-correlation function in productive and nonproductive layers

When comparing the correlation function results of elastic constants $C_{33}$and $C_{44}$ calculated in both productive and nonproductive layers, we notice that a difference exists and the correlation values for all components of elasticity tensor in productive layer are larger than those in nonproductive ones (Figures 14 and 15).

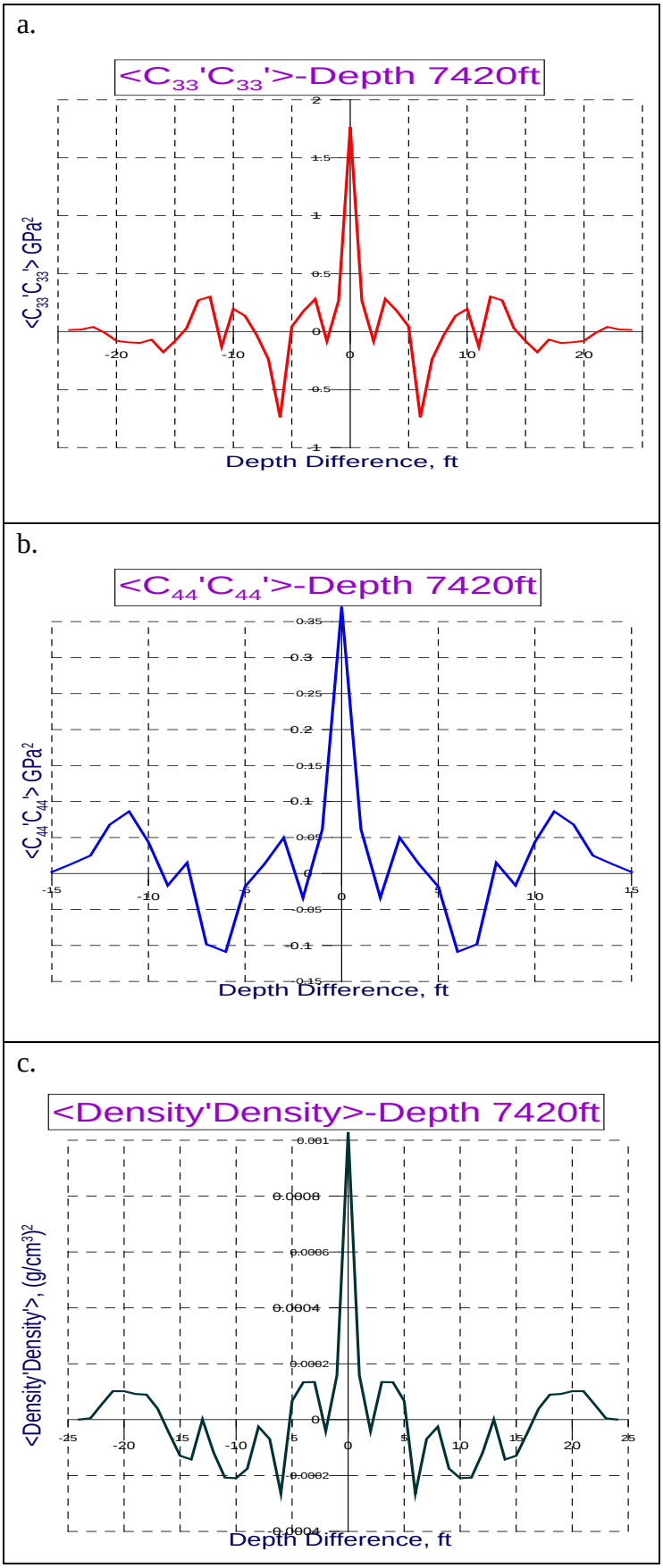


Figure 13: Pair-correlation functions for diverse elements of elasticity tensor and density constructed at 7420 ft depth, which is a nonproductive layer. Vp is 12054 ft/s; $Vs_1$ is 7552 ft/s. Frequency is 250 Hz.

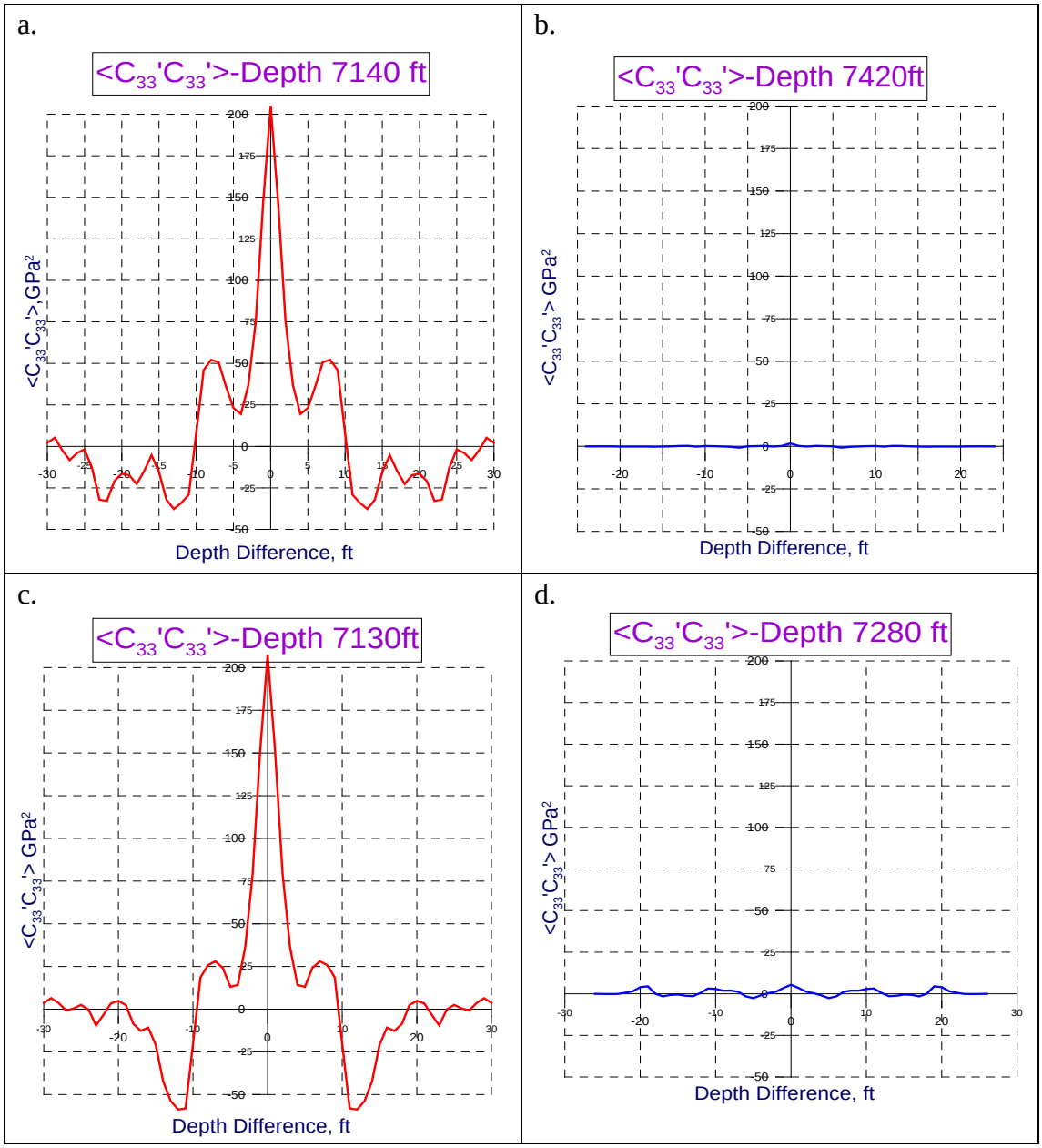


Figure 14: Correlation function is $< C'_{33}C'_{33} >$and frequency is 250 Hz: in (a) and (c), red lines represent the productive layers (Depth 7140 ft and Depth 7130 ft); in (b) and (d), the blue lines represent nonproductive layers (Depth 7420 ft and Depth 7280 ft).

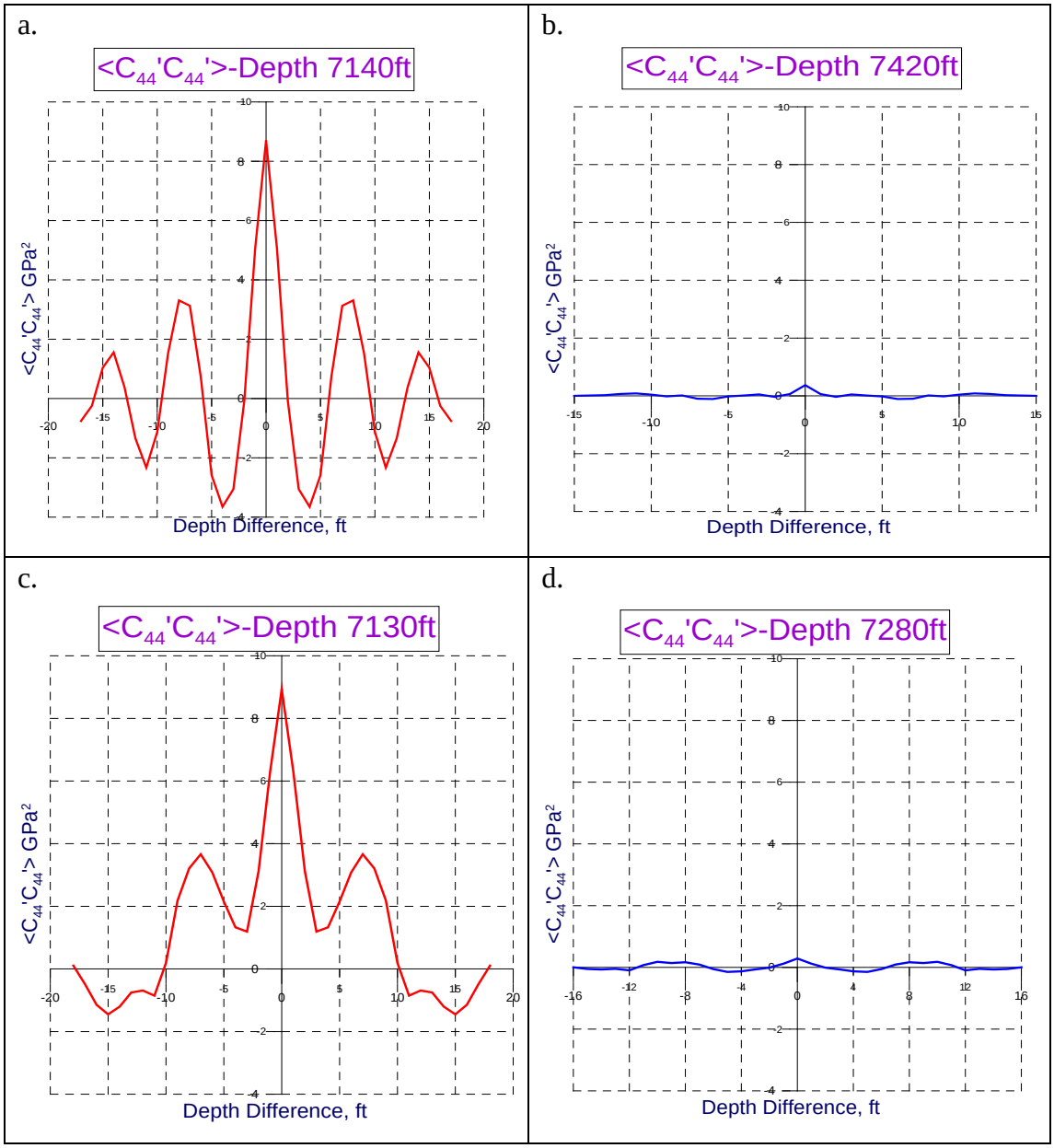


Figure 15: Correlation function is $<C'_{44}C'_{44}>$ and frequency is 250 Hz: in (a) and (c), the red lines are productive layers (Depth 7140 ft and Depth 7130 ft); in (b) and (d) the blue lines are non productive layers (Depth 7420 ft and Depth 7280 ft).

As a result, the increased heterogeneities caused by the gas/oil inclusions in the rock matrix enhance the difference between the effective and averaged elastic modulus. These productive layers with the enhanced difference exhibit greater pair correlation value than those nonproductive layers. Generally, the difference between the pair-correlation values computed for productive and non-productive layers are always greater than the difference for both productive and non-productive layers.

## 5.2. Amplitude of pair-correlation function versus depth

### 5.2.1 Using amplitude of pair-correlation function to identify the location of productive layers in productive well (Well 1)

In this section, we calculate and analyze the parameter of the pair-correlation function: amplitude. Amplitude is a very significant characteristic of correlation function and it can be applied to designate the locations for the productive layer. Commonly, the amplitude of correlation function reflects the inhomogeneity level of the medium. This means that the increased heterogeneity in the productive layer originates the maximum amplitude for pair-correlation function (Chesnokov, 2002). When the difference between the properties of the matrix and inclusion materials increases, the amplitude value becomes larger while the correlation radius decreases. For example, in a homogeneous medium with C(r) =const, the amplitude of correlation function is zero and the relative correlation radius is infinitely large. Therefore, the maximum amplitude of correlation function will indicate the productive layer of shale gas reservoir.

Figure 16 demonstrates the amplitudes of correlation function for various velocities ($Vp$, $Vs_1$, $Vs_2$), elasticity moduli and density, and confirms that the maximum amplitude correlates with the gas/oil reservoir location. Results are constant and prove that the maximum amplitude corresponds with the location of the productive layer. Therefore, for shale gas/oil reservoir, we can utilize the amplitudes of pair-correlation function as an indicator for the productive layer position.

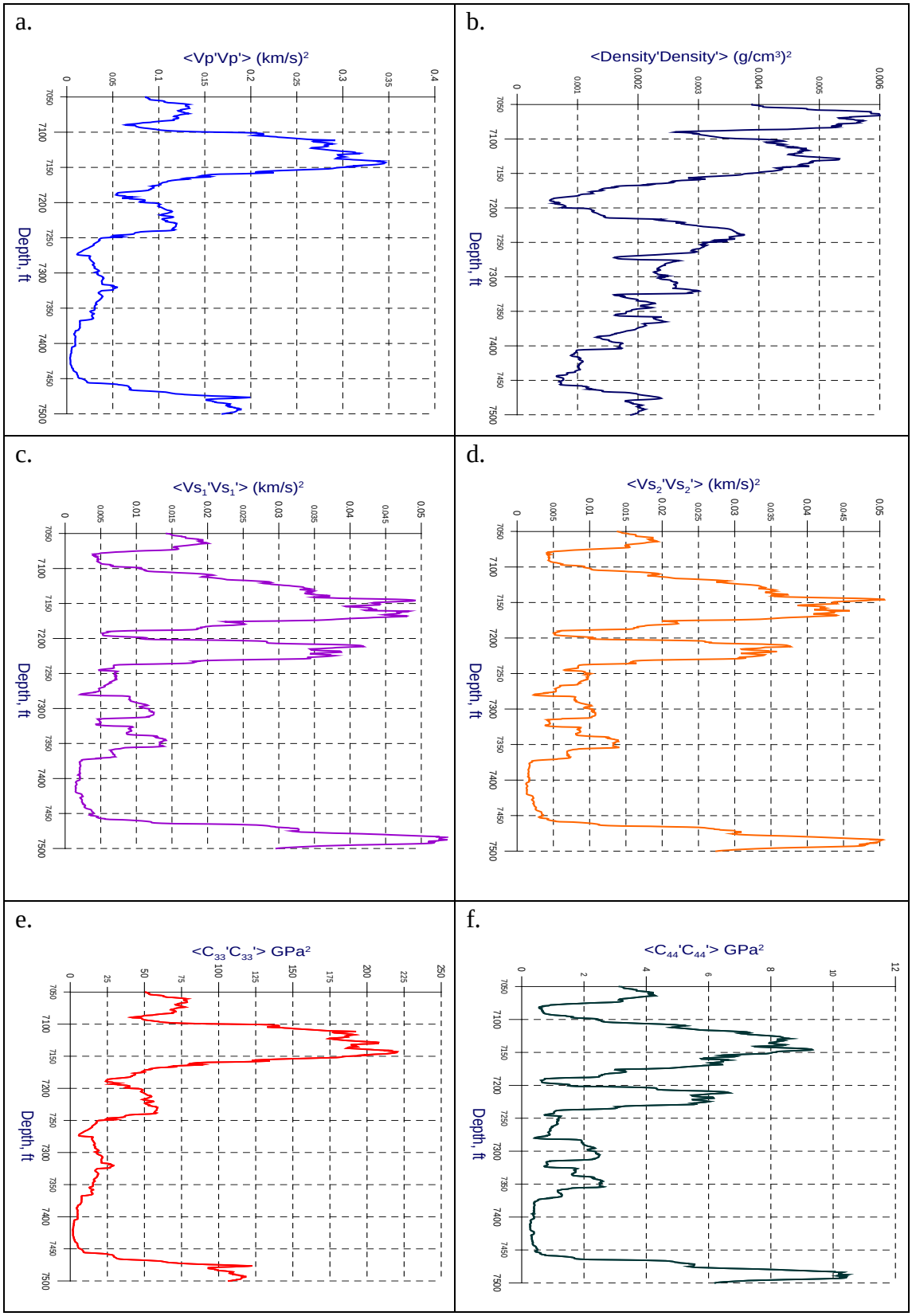


Figure 16: Amplitudes of pair-correlation function for the Barnett Shale based on the experimental log data from Well 1. Frequency is 250 Hz. (a) Amplitude of pair-correlation function $< V_P' V_P' >$. (b) Amplitude of pair-correlation function $< \rho' \rho' >$. (c) Amplitude of pair-correlation function $< Vs_1' Vs_1' >$. (d) Amplitude of pair-correlation function $< Vs_2' Vs_2' >$. (e) Amplitude of pair-correlation function $< C_{33}' C_{33}' >$. (f) Amplitude of pair-correlation function $< C_{44}' C_{44}' >$.

### 5.2.1 Using amplitude of pair-correlation function to distinguish productive wells from nonproductive wells

#### 5.2.1.a. Comparison of the amplitudes of the pair-correlation function for elasticity modules and density in a productive well (Well 1) and a nonproductive well (Well 2)

According to the conclusion we obtained from section 5.2.1, the amplitude of pair-correlation function can be utilized to point out the location of gas/oil reservoir for productive wells. We want to compare the amplitudes of pair-correlation function for both productive wells and nonproductive wells. Figure 17 displays the amplitudes of pair-correlation function for elasticity modules and density of the Barnett Shale based on the experimental log data from productive (Well 1) and nonproductive well (Well 2). The frequency we used is 250 Hz. The depth for Well 1 is from 7000 ft to 7500 ft; for Well 2, the depth is 7300 ft to 7500 ft. We observed that there was a great amplitude anomaly that existed in the depth of oil/gas reservoir location for productive well (Well 1), while the amplitude for nonproductive well (Well 2) was really small. Consequently, we can consider amplitude of pair-correlation function as an indicator to distinguish the productive wells from the nonproductive wells, because the difference between the inclusion and the material will result in the enhanced amplitude anomaly.

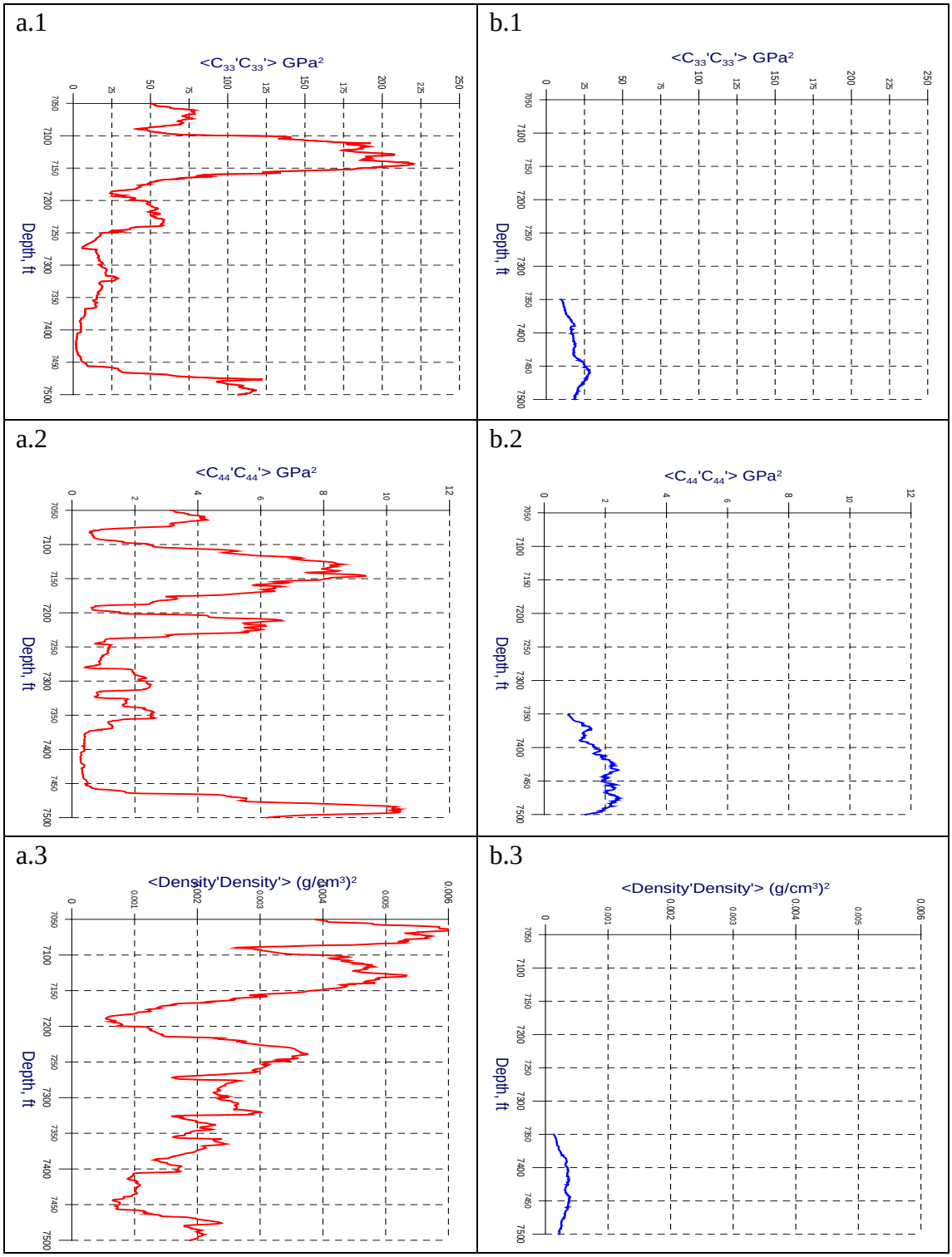


Figure 17: Amplitudes of pair-correlation function for elasticity modules and density of the Barnett Shale based on the experimental log data from Well 1 and Well 2. Frequency is 250 Hz. (a.1) Amplitude of pair-correlation function $< C'_{33}C'_{33} >$ for Well 1. (b.1) Amplitude of pair-correlation function $< C'_{33}C'_{33} >$ for Well 2. (a.2) Amplitude of pair-correlation function $< C'_{44}C'_{44} >$ for Well 1. (b.2) Amplitude of pair-correlation function $< C'_{44}C'_{44} >$ for Well 2. (a.3) Amplitude of pair-correlation function $< \rho'\rho' >$ for Well 1. (b.3) Amplitude of pair-correlation function $< \rho'\rho' >$ for Well 2.

### 5.2.1.b Comparison of the amplitudes of the pair-correlation function for elasticity modules and density in productive well (Well 1) and nonproductive wells (Well 3 and Well 4)

We also calculated and evaluated the amplitudes of pair-correlation function for both productive well (Well 1) and nonproductive wells (Well 3 and Well 4). Figure 18 presents the results and comparison between Well 1 and Well 3; Figure 19 refers to Well 1 and Well 4. The frequency is still 250 Hz. The depth scale for all wells is from 7000 ft to 7500 ft. The result for Well 1 reveals that the maximum of correlation amplitude is present in the depth of the productive layer. Nonetheless, the curves of amplitude versus depth for Well 3 and Well 4 also demonstrate great amplitude anomalies even though these two wells are nonproductive wells.

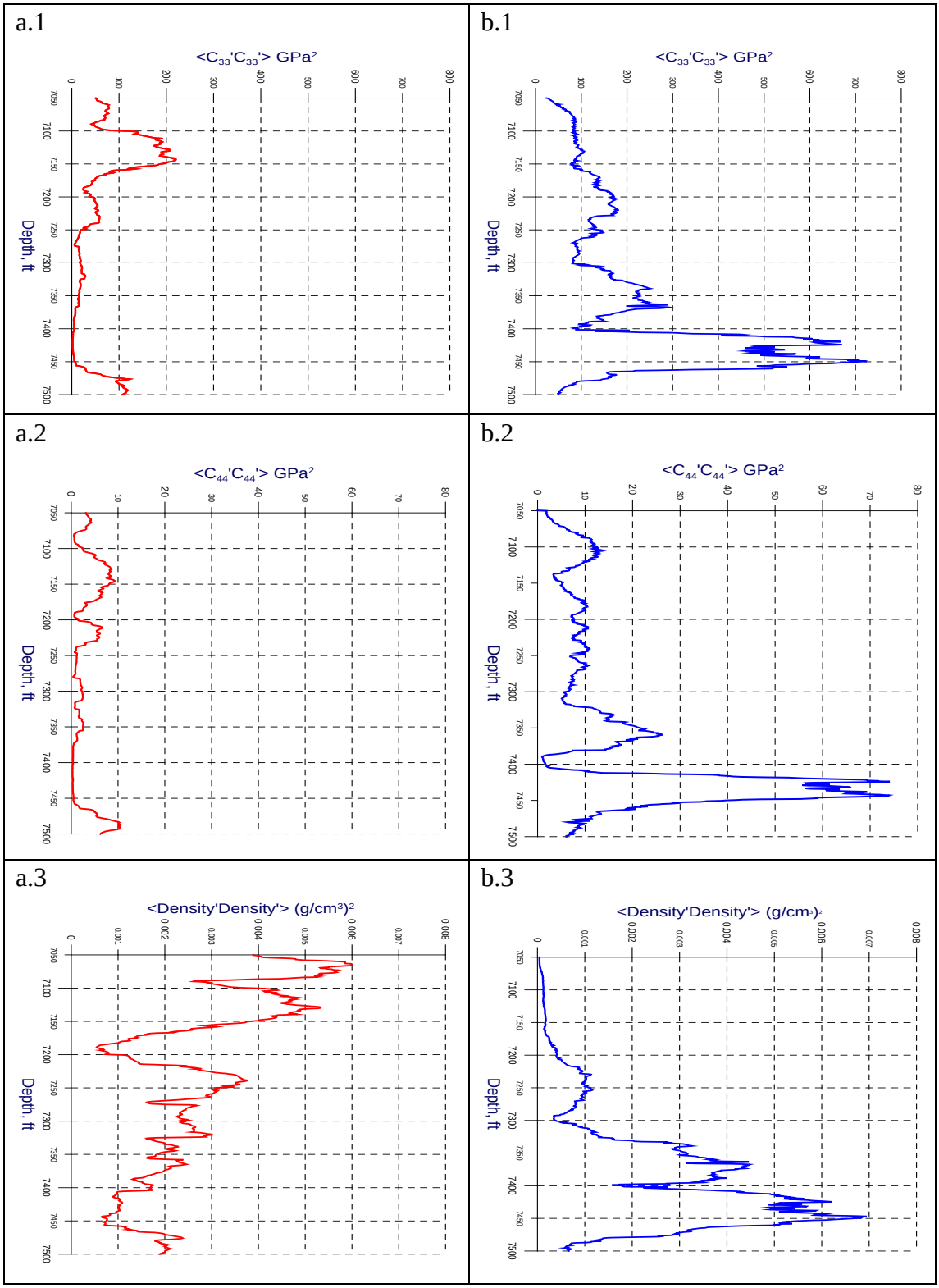


Figure 18: Amplitudes of pair-correlation function for elasticity modules and density of the Barnett Shale based on the experimental log data from Well 1 and Well 3. The frequency is 250 Hz. (a.1) Amplitude of pair-correlation function $< C'_{33}C'_{33} >$ for Well 1. (b.1) Amplitude of pair-correlation function $< C'_{33}C'_{33} >$ for Well 3. (a.2) Amplitude of pair-correlation function $< C'_{44}C'_{44} >$ for Well 1. (b.2) Amplitude of pair-correlation function $< C'_{44}C'_{44} >$ for Well 3. (a.3) Amplitude of pair-correlation function $< \rho'\rho' >$ for Well 1. (b.3) Amplitude of pair-correlation function $< \rho'\rho' >$ for Well 3.

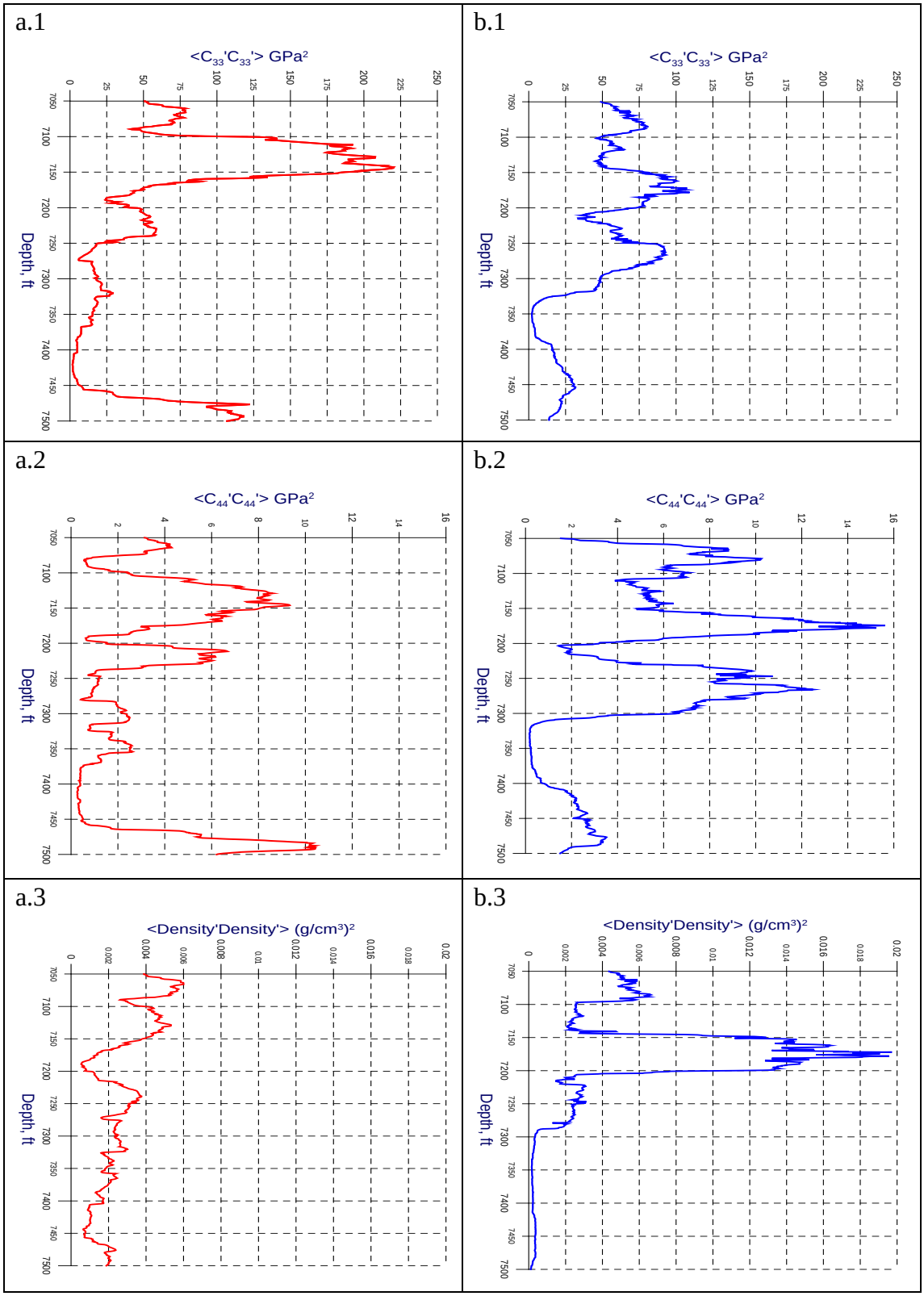


Figure 19: Amplitudes of pair-correlation function for elasticity modules and density about the Barnett Shale based on the experimental log data from Well 1 and Well 4. Frequency is 250Hz. (a.1) Amplitude of pair-correlation function $< C'_{33}C'_{33} >$ for Well 1. (b.1) Amplitude of pair-correlation function $< C'_{33}C'_{33} >$for Well 4. (a.2) Amplitude of pair-correlation function $< C'_{44}C'_{44} >$ for Well 1. (b.2) Amplitude of pair-correlation function $< C'_{44}C'_{44} >$ for Well 4. (a.3) Amplitude of pair-correlation function $< \rho'\rho' >$ for Well 1. (b.3) Amplitude of pair-correlation function $< \rho'\rho' >$ for Well 4.

Although analysis of these plots (Figure 18 and 19) suggests that the large amplitude abnormality of elasticity tensor reflects the distinction between the inclusions and the matrix rocks, they fail to explain whether these inclusions contain oil or gas. It means it is impossible for us to merely use amplitude of the pair-correlation function to discriminate gas/oil reservoir from other inclusions. For that reason, we combine the amplitude of pair-correlation function with Vp/Vs ratio together, and try to further analyze the results of the productive and nonproductive wells. Amplitudes of pair-correlation function for Vp/Vs ratio for both productive (Well 1) and nonproductive wells (Well 3 and Well 4) are presented in Figure 20. Results show significant differences in the correlation amplitudes for Vp/Vs ratio between the productive and nonproductive wells. For Well 1, we still find that the abnormal amplitudes exist and the layer with maximum value correlates with the depth location of the gas/oil layer. Conversely, there is no amplitude anomaly for both nonproductive wells and their amplitude values are extremely small compared with those of productive well.

In conclusion, the amplitude of pair-correlation function can reveal the presence of the inclusion in the materials, as well as differentiate the gas/oil inclusion from others with the analyses of Vp/Vs ratio. Therefore, we can develop amplitude of pair correlation function as a method:

1. to indentify the location of gas/oil reservoir for productive wells;
2. to distinguish productive wells from nonproductive wells.

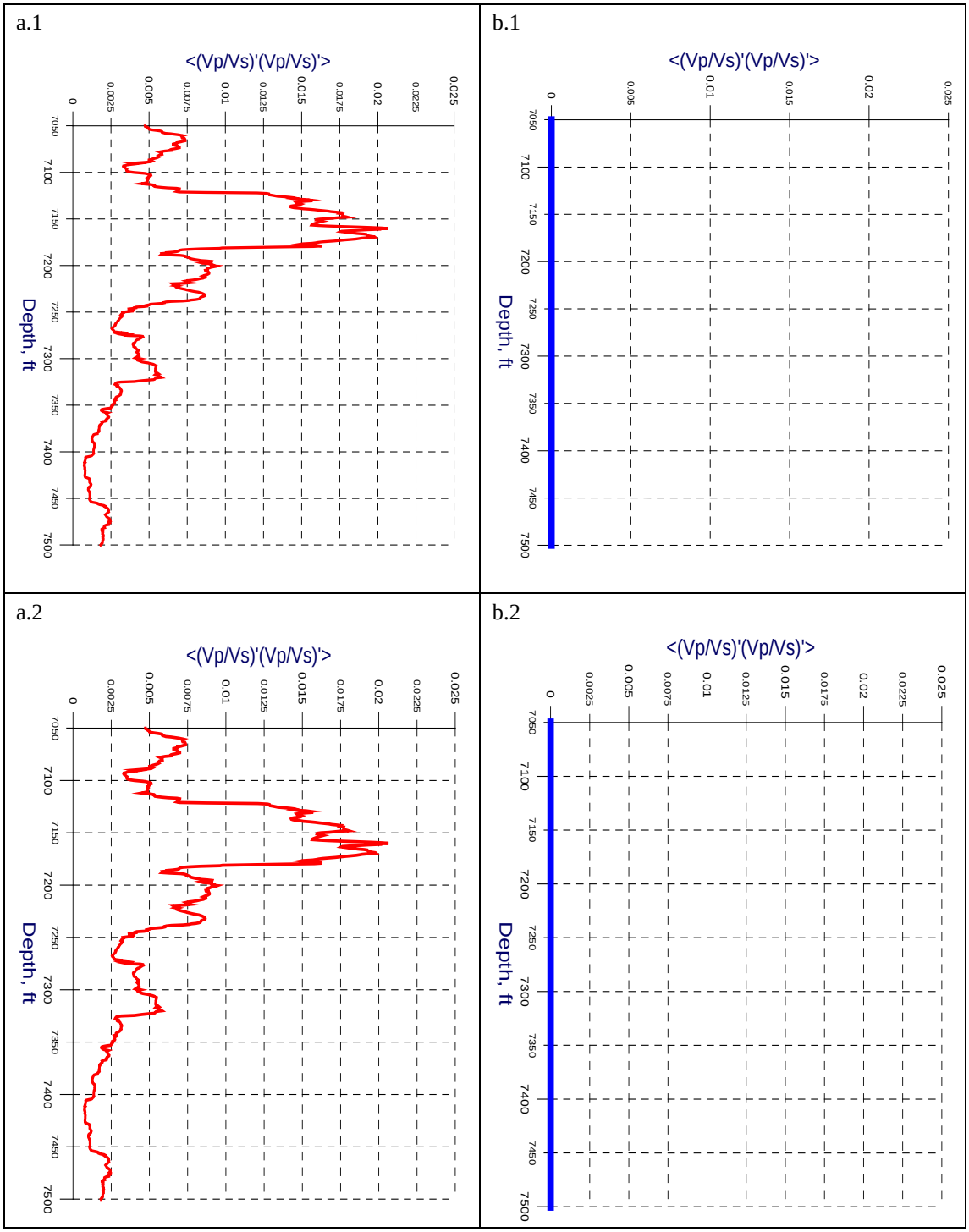


Figure 20: Amplitudes of pair-correlation function for Vp/Vs ratio about the Barnett Shale based on the experimental log data from productive well (Well 1) and nonproductive wells (Well 3 and Well 4). Frequency is 250 Hz. (a.1) Amplitude of pair-correlation function for Well 1. (b.1) Amplitude of pair-correlation function for Well 3. (a.2) Amplitude of pair-correlation function for Well 1. (b.2) Amplitude of pair-correlation function for Well 4.

## 5.3 Frequency-dependent amplitude of the pair-correlation function in productive well (Well 1)

Figure 21 illustrates the amplitudes of pair-correlation function $<C'_{33}C'_{33}>$ in diverse frequencies (100 Hz, 150 Hz, 250 Hz, 500 Hz, 1000 Hz, and 2000 Hz) for the productive well (Well 1). For the same productive layer, the decreasing in frequency results in the increasing of pair-correlation value and the relative amplitude, which can be an indication of enhanced heterogeneities. Heterogeneities can generate apparent anisotropy (Marson-Pidgeon and Savage, 1997), and previous studies show that anisotropy varies for different frequencies (Shapiro et al. 1994; Werner and Shapiro, 1999). When anisotropy becomes smaller with the increasing frequency (Liu, 2003), the fluctuation between the effective and averaged elasticity tensor also become smaller, which will cause a decrease in the amplitude of pair-correlation function.

Figure 22 shows the amplitude of pair-correlation function for $<C'_{33}C'_{33}>$. The depth scale is from 7000 ft to 7500 ft and the frequency scale is from 100 Hz to 1000 Hz. The result demonstrates that the highest amplitude value exists at the productive layers with the frequency at 100 Hz and the amplitudes decrease with the increasing of the frequency. Whereas, for nonproductive layers, the amplitudes are small and almost keep constant when the frequency increases. As a result, for a heterogeneous medium, calculated results suggest that pair-correlation function and its amplitude essentially depend on frequency.

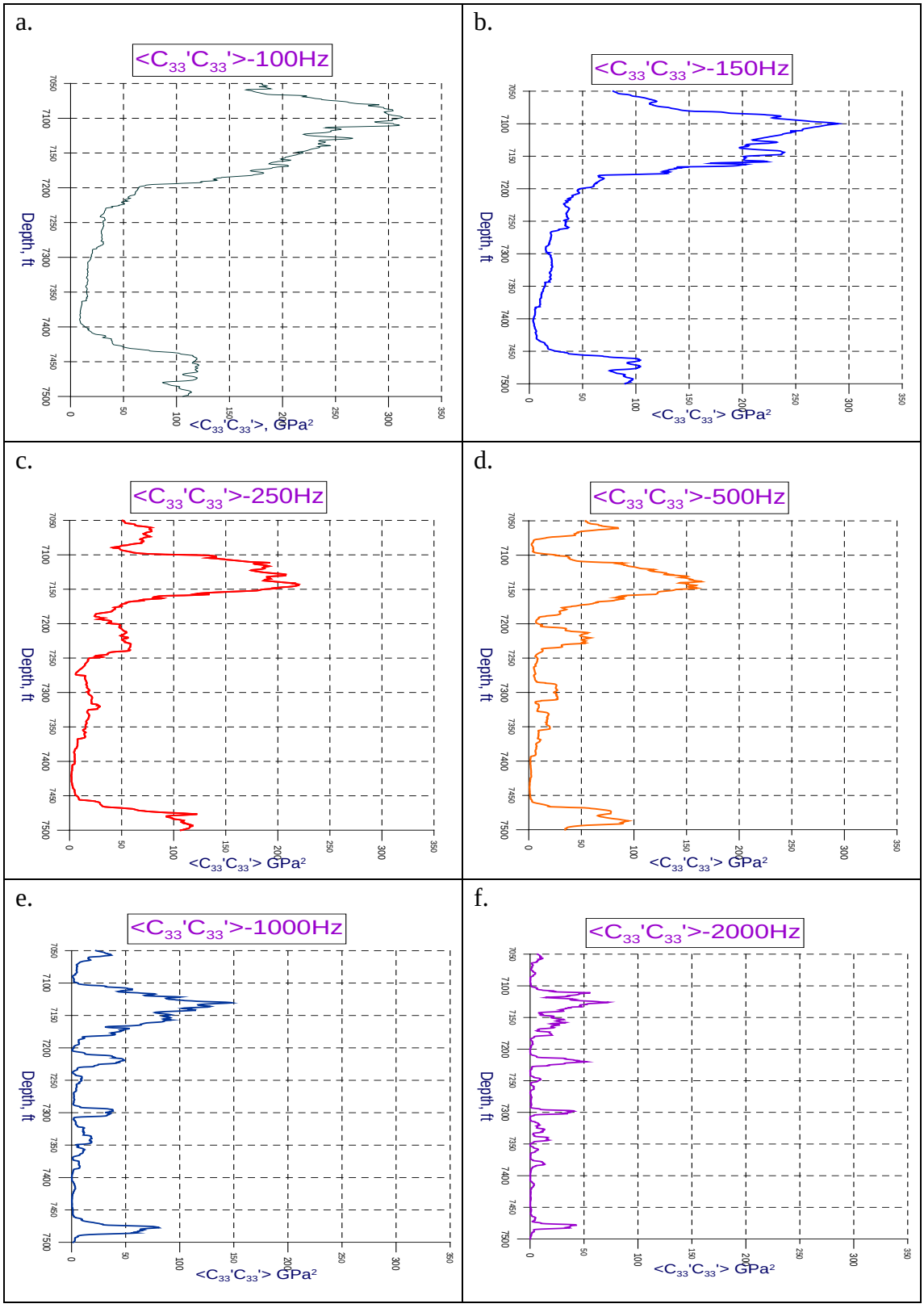


Figure 21: Amplitudes of pair-correlation function $< C'_{33}C'_{33} >$ for the Barnett Shale based on the experimental log data from Well 1. (a) Amplitude of pair-correlation function $< C'_{33}C'_{33} >$ at 100 Hz. (b) Amplitude of pair-correlation function $< C'_{33}C'_{33} >$ at 150 Hz. (c) Amplitude of pair-correlation function $< C'_{33}C'_{33} >$ at 250 Hz. (d) Amplitude of pair-correlation function $< C'_{33}C'_{33} >$ at 500 Hz. (e) Amplitude of pair-correlation function $< C'_{33}C'_{33} >$ at 1000 Hz. (f) Amplitude of pair-correlation function $< C'_{33}C'_{33} >$ at 2000 Hz.

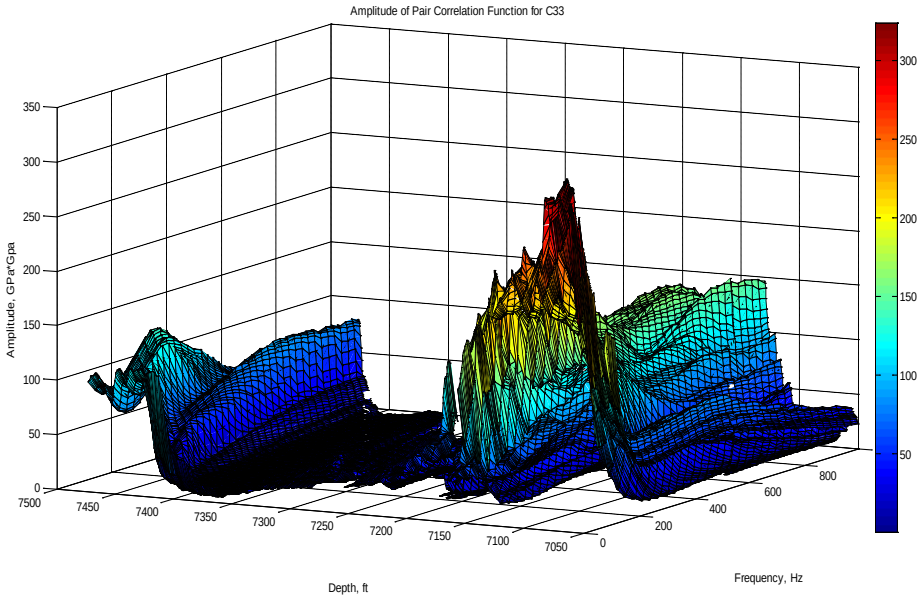


Figure 22: Amplitude of pair-correlation function $< C'_{33}C'_{33} >$ for productive well (Well 1) in the frequency scale (100 Hz to 1000 Hz).

Figure 23 illustrates the amplitudes of pair-correlation function calculated in a variety of frequencies (100 Hz, 150 Hz, 250 Hz, 500 Hz, 1000 Hz, and 2000 Hz) for two specific depths. The red line represents the depth of 7140 ft, which are the productive layers, and blue symbolizes the depth of 7420 ft, which are the nonproductive layers. According to these results, we perceive that the amplitudes for the productive layer are always bigger than the nonproductive layers. For productive layers, the differences between amplitude calculated in diverse frequencies are bigger and amplitudes decrease quickly with the increase of frequency. The results demonstrate that the amplitudes of correlation function dramatically change with the frequency at productive layers. For nonproductive layers, after certain frequencies, the amplitudes of pair-correlation function become constant and their changes with increasing frequency becomes really small. Hence, this suggests that for a

homogeneous medium, the amplitude of pair-correlation function will remain constant and pair-correlation function for elastic modulus will be independent of frequency.

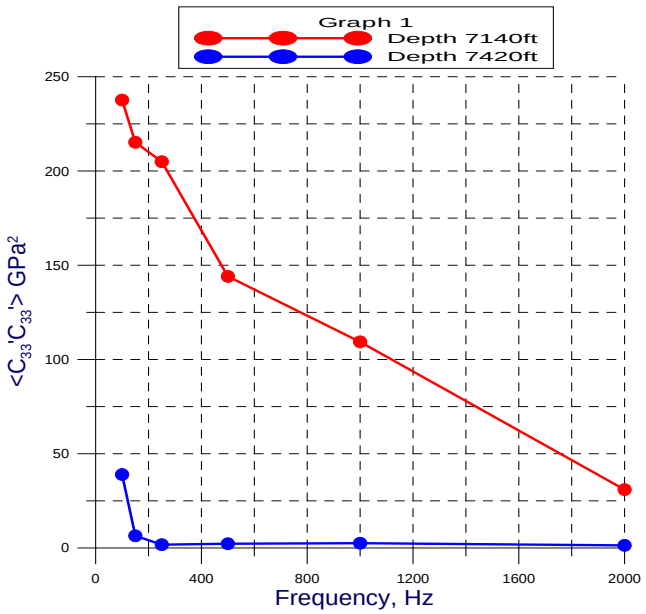


Figure 23: Amplitude of pair-correlation function $< C'_{33}C'_{33} >$ in diverse frequency (100 Hz, 150 Hz, 250 Hz, 500 Hz, 1000 Hz, 2000 Hz) for a certain depth. The red line represents the productive layer-7140 ft; the blue line symbolizes the nonproductive layer-7420 ft. Solid circled points stand for amplitude value for each given frequency.

# Chapter 6 Summary

We utilized the pair-correlation function method developed by Dr. Chesnokov et.al. (2001) to calculate the experimental data from four different well logs and predict the physical characteristics for the Barnett Shale. We estimated the components of elasticity tensor based on the sonic log data and density log data. Afterwards, we computed the pair-correlation function for various elastic modulus and density in different frequency domains, and then calculated and analyzed their relative amplitudes. Based on the calculated results and analyses, we concluded that,

1. For productive wells, there are differences between the pair-correlation values for productive layers and non-productive layers. Productive layers exhibit higher correlation values because of the larger difference between the effective and averaged elasticity tensor. The heterogeneity of the material (the inclusion among the matrix rocks) enhances the difference. Generally, the difference between the pair-correlation values computed for productive and non-productive layers are always greater than the difference for both productive and non-productive layers. Therefore, the layers of higher pair-correlation values correlate with depth location of shale oil/gas reservoir.
2. Calculated results of pair-correlation function for diverse elastic wave velocities ($Vp, Vs_1, Vs_2$), elasticity tensor factors ($C_{33}$, $C_{44}$) and density $\rho$ in different frequencies prove they are frequency-dependent due to the increased scattering

caused by the enhanced heterogeneities of the medium. Results demonstrate that pair-correlation values for low frequency is greater than one for high frequency at the same depth. Conversely, pair-correlation function in higher frequency can reveal more features of their physical characteristics. In addition, the difference between the pair-correlation function calculated in different frequencies for productive layers are larger than the difference for nonproductive layers. This means that the pair-correlation values and its relative amplitudes for productive layers decrease more rapidly with the increasing of the frequency. For the nonproductive layer, after a certain frequency, the amplitudes of pair-correlation function become constant and their changes with increasing frequency becomes very small. Therefore, this suggests that for a homogeneous medium, the amplitude of pair-correlation function will stay constant and pair-correlation function for elastic modulus will become independent of frequency. For heterogonous medium, the pair-correlation function is frequency-dependent because of frequency-dependent anisotropy. For lower frequency, the ratio between the wavelength and the size of inclusion increases, which causes the enhanced magnitude of heterogeneity, thus the calculated pair-correlation value will be large.

3. Amplitude of the pair-correlation function is one of its significant parameters. Correlation amplitude reflects the level of inhomogeneity of a medium. Higher amplitude anomaly indicates the increased contrast between the inclusion and the medium. Commonly, the maximum correlation amplitude and the minimum

correlation radius are associated with the depth location of productive layers. As a result, without knowing the exact depth position of shale oil/gas reservoir, we can use pair-correlation amplitude as an indicator to predict the productive layers and to estimate the thickness of the productive layers.

4. The compared results between productive well (Well 1) and non-productive wells (Well 3 and Well 4) show that we cannot simply rely on amplitude of pair-correlation function for elastic modulus as a tool to distinguish the productive wells from non-productive ones. However, combined with the analysis of Vp/Vs ratio, we improve the pair-correlation function method. Compared with the correlation amplitude for elements of elastic tensor and density, amplitude of correlation function for Vp/Vs ratio is a better index to divide the productive and non-productive wells.

# References

Bayuk, I. O., M. Ammerman, and E. M. Chesnokov, 2008, Upscaling of elastic properties of anisotropic sedimentary rocks: Geophysical Journal International, 172, 842–860.

Bayuk, I. O., A. A. Vikhorev, J. M. Hooper, V. V. Tertychnyi, Y. A. Kukharenko, and E.M. Chesnokov, 2003, Frequency dependent effects in porous rocks: International Conference and Exhibition, EAEG, Extended Abstracts, PS10.

Chesnokov, E. M., 2002, Correlation Function as a Tool to Recognize the Productive Layers: $8^{th}$ European Conference on the Mathematics of Oil Recovery, 8 p.

Chesnokov, E. M., A, K, Yuri, and I. O. Bayuk, 2001, Mathematical modeling the frequency dependence of velocities in random media based on well log and seismic data.: United institute of physics of the earth Russian academy of sciences, Laboratory of Geophysics of Ordered Media Rock Physics and Reservoir Structure Monitoring Project, Norman, Ponca City, Moscow, 155p.

Chesnokov, E.M., J.H. Queen, Y. A. Kukharenko, J. M. Hooper, and I.O. Bayuk, 2000, Dispersive Properties of Porous Cracked Media: Proceedings of the 7th European Conference on the Mathematics of Oil Recovery, 5-8 September, Baveno, Italy.

Chesnokov, E.M., J.H. Queen, A.A.Vichorev, H.B. Lynn, J.M. Hooper, I.O. Bayuk , J. A. Castagna and B. Roy, 2001, Frequency Dependent Anisotropy: SEG, 2001, ANI 1.9. San Antonio.

Chesnokov, E. M., and Y. A. Kukharenko, 1996, Tensor of effective density for media with inclusions: 66th Annual International Meeting, SEG, Expanded Abstracts, 1033–1036.

Chesnokov, E. M., Y. A. Kukharenko, and P. A. Kukharenko, 1995, Method of diagram technique for calculation of effective physical parameters of microinhomogeneous media: SPIE—International Society of Optical Engineers, Mathematical Methods in Geophysical Imaging III, 2–12.

Chesnokov, E. M., Y. A. Kukharenko, and P. Y. Kukharenko, 1998, Frequency Dependence of Physical Parameters of Microinhomogeneous Media, Space Statistics: Revue Del' Institut Francais Du Petrole, v. 53, no. 5, p. 729-734.

Glorioso, J. C., A. Rattia, and Repsol, 2012, Unconventional Reservoirs: Basic

Petrophysical Concepts for Shale Gas: SPE 153004, 38p.

Leckie, D. A., C. Singh, F. Goodarzi, and J. H. Wall, 1990, Organic-rich, radioactive marine shale: A case study of a shallow-water condensed section, Cretaceous Shaftesbury Formation, Alberta, Canada: Journal of Sedimentary Petrology, v. 60, no. 1, p. 101–177.

Liu, E., J.H. Queen, X.Y. Li, M. Chapman, S. Maultzsch, H.B. Lynn, and E.M. Chesnokov, 2003, Observation and analysis of frequency-dependent anisotropy from a multicomponent VSP at Bluebell-Altamont Field, Utah: Journal of Applied Geophysics, v. 54, p. 319-333

Lu, K. F., 2012, Gas Shale Permeability and Velocity Measurement at Laboratory Scale: M. Sc. thesis, University of Houston, Texas, U.S.A., 62p.

Martineau, D. F., 2007, History of the Newark East field and the Barnett Shale as a gas reservoir: AAPG Bulletin, v. 91, no. 4, p. 399-403.

Marson-Pidgeon, K., Savage, M.K., 1997. Frequency-dependent anisotropy in Wellington, New Zealand: Geophys. Res. Lett. 24 (24), 3297– 3300.

Montgomery, S. L., D. M. Jarvie, K. A. Bowker, and R. M. Pollastro, 2005, Mississippian Barnett Shale, Fort Worth basin, north-central Texas: Gas-shale play with multi–trillion cubic foot potential: AAPG Bulletin, v. 89, no. 2, p. 155-175.

Pettijohn, F.J., 1975, Sedimentary rocks, 3rd Edition, pp. 260 - 265.

Ross, D. J. K., and R. M. Bustin, 2008, Characterizing the shale gas resource potential of Devonian–Mississippian strata in the Western Canada sedimentary basin: Application of an integrated formation evaluation: AAPG Bulletin, v. 92, no. 1, p. 87-125.

Roy, B., J. Queen, I. O. Bayuk, Y. A. Kukharenko, and E. M. Chesnokov, 2001, Prediction of frequency dependent velocity in porous reservoir: 71st Annual International Meeting, SEG, ExpandedAbstracts, 1933–1936.

Shapiro, S.A., Zien, H., Hubral, P., 1994. A generalised O'Doherty-Ansley formula for waves in finely layered media: Geophysics, v. 59, p.1750– 1762.

Shermergor, T. D., 1977, Theory of elasticity of microinhomogeneous media: Nauka _in Russian.

Slatt, R. M., and Y. Abousleiman, 2011, Merging sequence stratigraphy and geomechanics for unconventional gas shales: The Leading Edge, 30, 274–282.

Slatt, R. M., and N. R. O'Brien, 2011, Pore types in the Barnett and Woodford gas shales: Contribution to understanding gas storage and migration pathways in fine-grained rocks: AAPG Bulletin, 95, no.12, 2017–2030.

Tiwary, d. k. , I. O. Bayuk, A. A. Vikhorev, and E. M. Chesnokov, 2009, Comparison of seismic upscaling methods: From sonic to seismic: GEOPHYSICS, v. 74, no. 2, p.WA3–WA14.

Werner, U., Shapiro, S.A., 1999. Frequency-dependent shear-wave splitting in thinly layered media with intrinsic anisotropy: Geophysics, v. 64, p. 604–608.